AD-A250 738

AFOSR-TR- 92 0036

②

DTIC
ELECTE
MAY 18 1992
S D

Final Report Submitted to the Air Force Office of Scientific Research:

Backward-Wave Oscillator Investigations in the Raman Regime

(Grant AFOSR-89-0393E)

---

29 February 1992

Edl Schamiloglu & John Gahl, Assistant Professors
Pulsed Power & Plasma Science Laboratory

Department of Electrical and Computer Engineering
University of New Mexico
Albuquerque, NM   87131

AIR FORCE OF SCIENTIFIC RESEARCH (AFSC)

reviewed and is
IAW AFR 190-12

92-13070

02 5 15 033

REPORT DOCUMENTATION PAGE

Public reporting burden for this collection of information is estimated to average 1 hour per response, including the time for reviewing instructions, searching existing data sources, gathering and maintaining the data needed, and completing and reviewing the collection of information. Send comments regarding this burden estimate or any other aspect of this collection of information, including suggestions for reducing this burden, to Washington Headquarters Services, Directorate for Information Operations and Reports, 1215 Jefferson Davis Highway, Suite 1204, Arlington, VA 22202-4302, and to the Office of Management and Budget, Paperwork Reduction Project (0704-0188), Washington, DC 20503.

1. AGENCY USE ONLY (Leave blank)	2. REPORT DATE	3. REPORT TYPE AND DATES COVERED
	29 Feb 92	Final Report 01Aug89-31Dec91

4. TITLE AND SUBTITLE	5. FUNDING NUMBERS
Backward-Wave Oscillator Investigations in the Rama Regime	2301/A8

6. AUTHOR(S)

Professors Edl Schamiloglu & John Gahl

7. PERFORMING ORGANIZATION NAME(S) AND ADDRESS(ES)	8. PERFORMING ORGANIZATION REPORT NUMBER
Dept of Electrical & Computer Engrg University of New Mexico Albuquerque, NM 87131	AFOSR-TR 92 0266

9. SPONSORING/MONITORING AGENCY NAME(S) AND ADDRESS(ES)	10. SPONSORING/MONITORING AGENCY REPORT NUMBER
AFOSR/NE Bldg 410 Bolling AFB DC 20332-6448 Dr Barker	AFOSR-89-0393

11. SUPPLEMENTARY NOTES

12a. DISTRIBUTION/AVAILABILITY STATEMENT	12b. DISTRIBUTION CODE
UNLIMITED	

13. ABSTRACT (Maximum 200 words)

The Univ of New Mexico short-pulse backward-wave oscillator (BWO) experiment utilizes a 600-700 keV, 1-4 KA electron beam to generate microwave radiation due to the interaction with sinuoidally-rippled wall slow wave structures.   (SEE REPORT FOR DETAILS)

14. SUBJECT TERMS	15. NUMBER OF PAGES
	16. PRICE CODE

17. SECURITY CLASSIFICATION OF REPORT	18. SECURITY CLASSIFICATION OF THIS PAGE	19. SECURITY CLASSIFICATION OF ABSTRACT	20. LIMITATION OF ABSTRACT
UNCLASSIFIED	UNCLASSIFIED	UNCLASSIFIED	

NSN 7540-01-280-5500

Table of Contents

I. Executive Summary

The University of New Mexico short-pulse backward-wave oscillator (BWO) experiment utilizes a 600-700 keV, 1-4 kA electron beam to generate microwave radiation due to the interaction with a sinusoidally-rippled wall slow wave structure. The results of the experiment are:

1. there is no evidence of dominant mode TM_{01} microwave generation

2. there is evidence of second order TM_{02} microwave generation

3. there is also evidence of TE-like microwave generation, probably due to electron beam disruption, in competition with the BWO-generated microwaves

4. the microwave power generated in the 22-27 GHz region is in the 0.01-0.1 MW range

A linear calculation of the dispersion relation for the slow-wave structures, including the effects of beam space charge, is consistent with the data indicating higher-order mode operation of the experiment. MAGIC simulations indicate dominant mode operation, though the simulations utilized idealized voltage profiles. The TE-like microwaves are probably due to a beam rotation-induced instability causing the electron azimuthal distribution to breakup. The effects of a triangular voltage pulse distribution are being investigated in the context of a recent theoretical model proposed by researchers at the University of Maryland.

This final report is organized as follow. Section II provides a brief description of the UNM short-pulse BWO experimental hardware. The linear theory of the device and electromagnetic simulation results are described in Sec. III. The experimental results indicating the generation of microwave radiation under varying parameters is presented in Sec. IV. Experimental tasks, in addition to short-pulse microwave generation, are discussed in Sec. V. Preliminary conclusions regarding microwave generation are presented in Sec. VI. (A more complete description and presentation of the UNM short-pulse BWO experimental results will be forthcoming in a M.S. thesis to be completed in the Spring 1992 semester.) Future plans of the UNM BWO

group are summarized in Sec. VII. References for this document are contained in Sec VIII. Finally, the Appendices contain additional information relevant to the past grant period.

II. Brief Description of the UNM Short-Pulse BWO Experiment

Electron Beam Accelerator

The University of New Mexico (UNM) short-pulse backward-wave oscillator (BWO) experiment was designed to generate high-power Ku-band microwave radiation in a 15 ns pulse width. A modified Nereus[1] Marx generator and an oil-filled Blumlein transmission line are used to produce an electron beam which feeds into a slow-wave structure to produce microwave radiation (Fig. 1).

The modified Marx bank is a 3.75 kJ, 600 kV, oil-insulated generator that has twelve 50 kV, 0.25 μF capacitors arranged in an $n = 2$ plus-minus charged configuration. In the first stage of operation, the capacitors are charged in parallel and discharged in series. In a typical shot, the capacitors are slowly charged to 35-40 kV through a large charging resistor (R_h in Fig. 2). The capacitors are then switched ("erected") into a series configuration by triggering the spark gaps. There are 6 spark gaps in the Marx tank that are housed in two acrylic tubes pressurized with commerical dry air to about 40 psig. Each spark gap consists of a pair of 6.35 cm diameter brass spheres with a separation of about 1.6 cm. The first gap in each tube has a needle inserted between the spheres to initiate breakdown. The spark gaps are closed for a period of time that is much less than the time constant of the capacitors and the charging resistors, resulting in little loss through the charging circuit. After the spark gaps are triggered, the Marx bank circuit is equivalent to a single capacitor with twelve times the charge voltage and one twelfth the capacitance. The trigger circuit is a series combination of "door knob" capacitors and a Pacific-Atlantic Trading Company PT-55 high voltage pulser. The transfer of energy to the Blumlein transmission line is the second stage of operation.

The Blumlein (Fig. 3(a)) is an oil-filled transmission line which compresses the erected Marx voltage pulse from about 1 μs to about 16 ns. There are two coaxial transmission lines nested inside one another, each having an impedance of about 18 Ω. The load impedance for the Blumlein is the electron beam diode, which is connected across the inner and outer conductors (Fig. 3(b)). In order to match the transmission line to the high impedance electron diode load, a pair of sodium
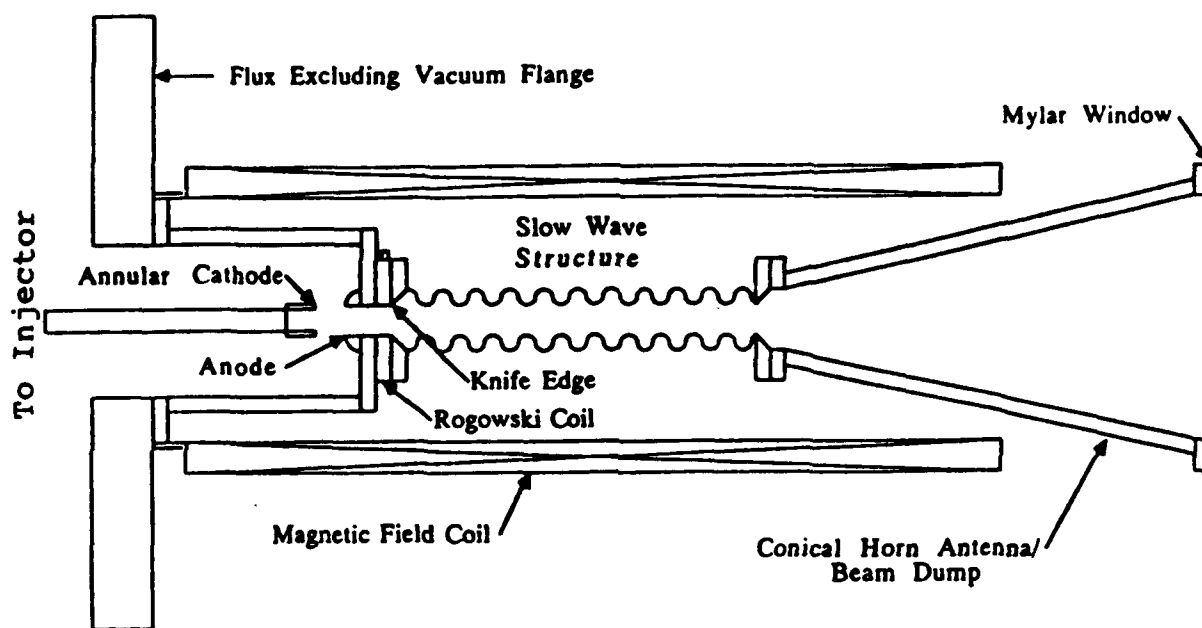
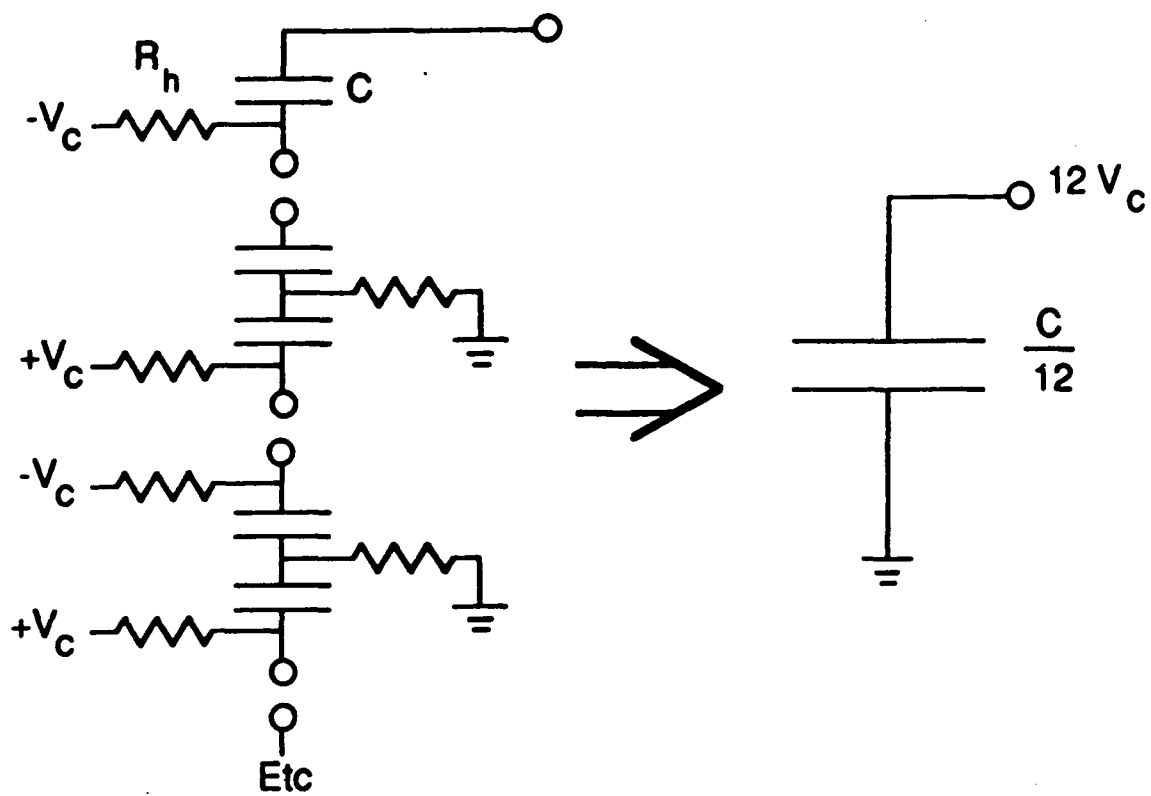FIG. 1. The main components of the UNM short-pulse BWO experiment.

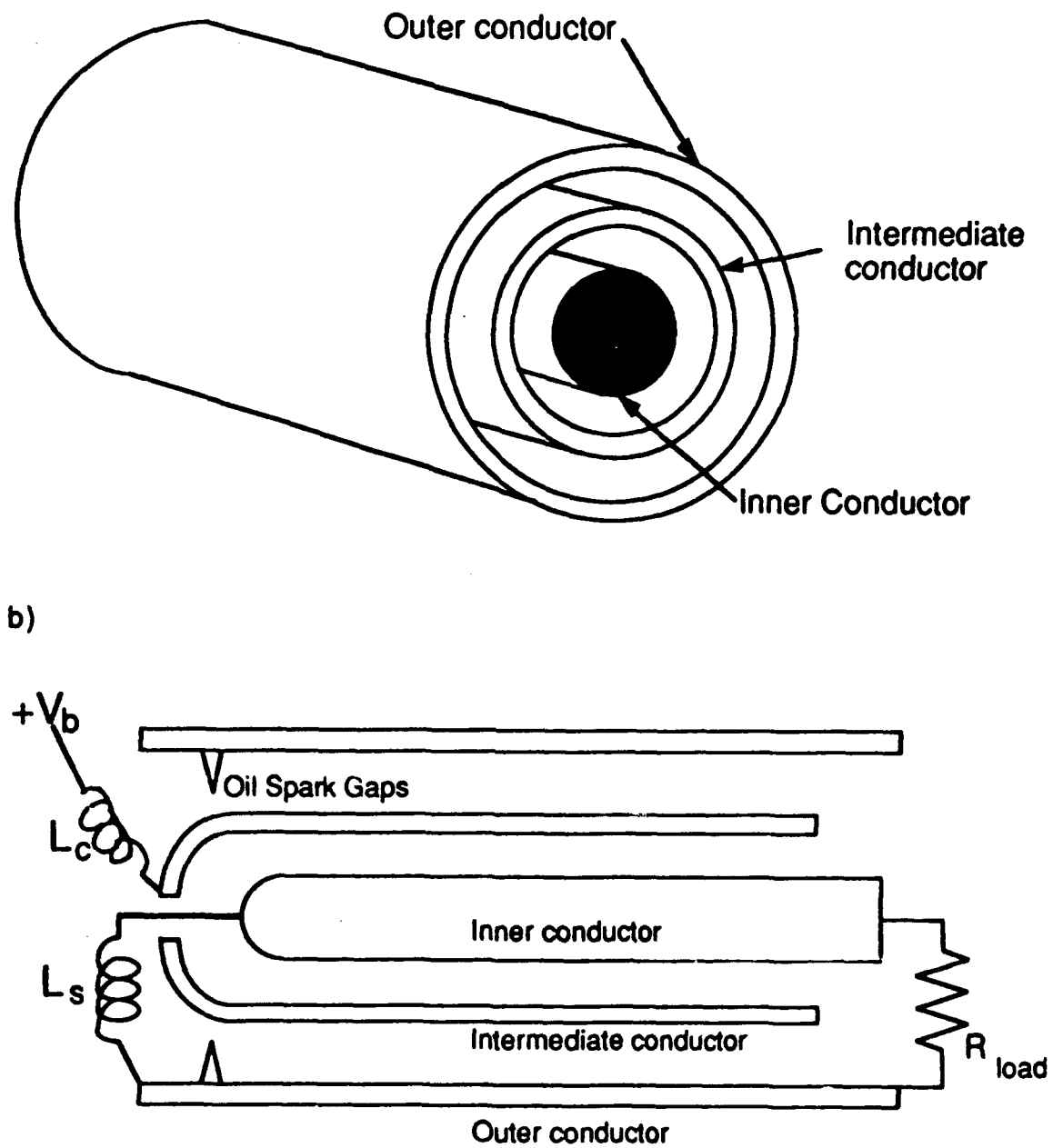FIG. 2. Diagram of the erected modified Nereus Marx generator.

FIG. 3. The Blumlein transmission line configuration: a) nested conductors, and b) schematic of connections.

thiosulfate resistors were installed parallel to the diode near the oil-vacuum interface. These resistors were later removed since they also limited the current in the diode anode-cathode $(A - K)$ gap. The resultant voltage reflections on the transmission line did not severely disrupt the operation of the electron beam generator.

The Marx bank is connected to the intermediate conductor at the input end of the Blumlein transmission line through a charging inductor L_c (Fig. 4(b)). As the Marx bank charges the intermediate conductor, the inner conductor is prevented from floating up in voltage by a shorting inductor L_s (Fig. 4(b)). Four oil-immersed spark gaps are arranged around the perimeter of the input end of the outer transmission line to provide a current path across the outer-intermediate conductor gap. The oil gaps are set to self-break when the Blumlein voltage reaches the desired output voltage. The diode then "sees" the Blumlein voltage for twice the transit time of a pulse down the transmission line. The advantage of using a Blumlein transmission line is that the full charge voltage appears across the load.[2] Recent diode voltage and current pulses obtained without the parallel matching resistors are shown in Fig. 4.

The voltage is finally delivered to a Poco graphite cathode of 7.43 mm radius (cathode #9 in our notation) mounted on a 21.0 cm long brass stalk. The stalk serves two purposes. First, it enables the $A - K$ to be adjustable so that the beam current may be varied (the anode position is fixed in the experiments). Second, the stalk ensures that the beam electrons are born in a region of uniform longitudinal guide magnetic field. As will be seen later, a strong magnetic field is required to guide the electron beam in vacuum through the slow-wave structures.

Magnetic Field-Producing Coil

The magnetic field coil was designed to produce a uniform field at the axial position where electrons are "born"-a field-immersed geometry for the cathode. This is evident in Fig. 5(a), where the positions of the anode and cathode are denoted on an experimentally measured axial field profile.

To achieve the intense magnetic field, a solenoidal coil, powered by a pair of 500 mF, 10 kV capacitors, was constructed. The capacitors are switched by a NLS553B ignitron and discharged on command through the coil. A typical current response is shown in Fig. 5(b) and can be seen to reach a maximum strength at
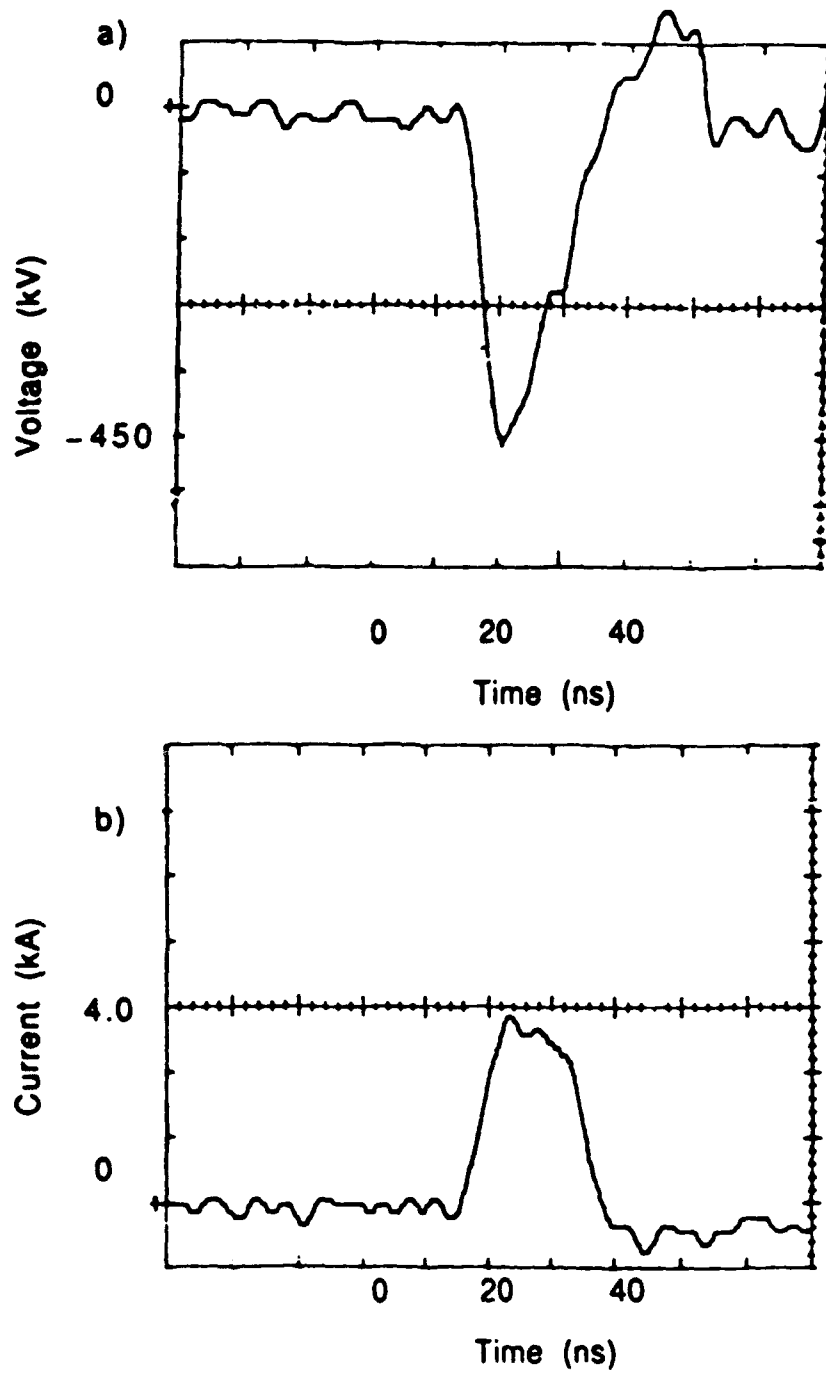
FIG. 4. Typical diode traces: a) voltage, and b) current.

a)

A-K Gap

(Graph of Magnetic Field (Tesla) vs Position (mm relative to anode))

Position (mm relative to anode)

b)

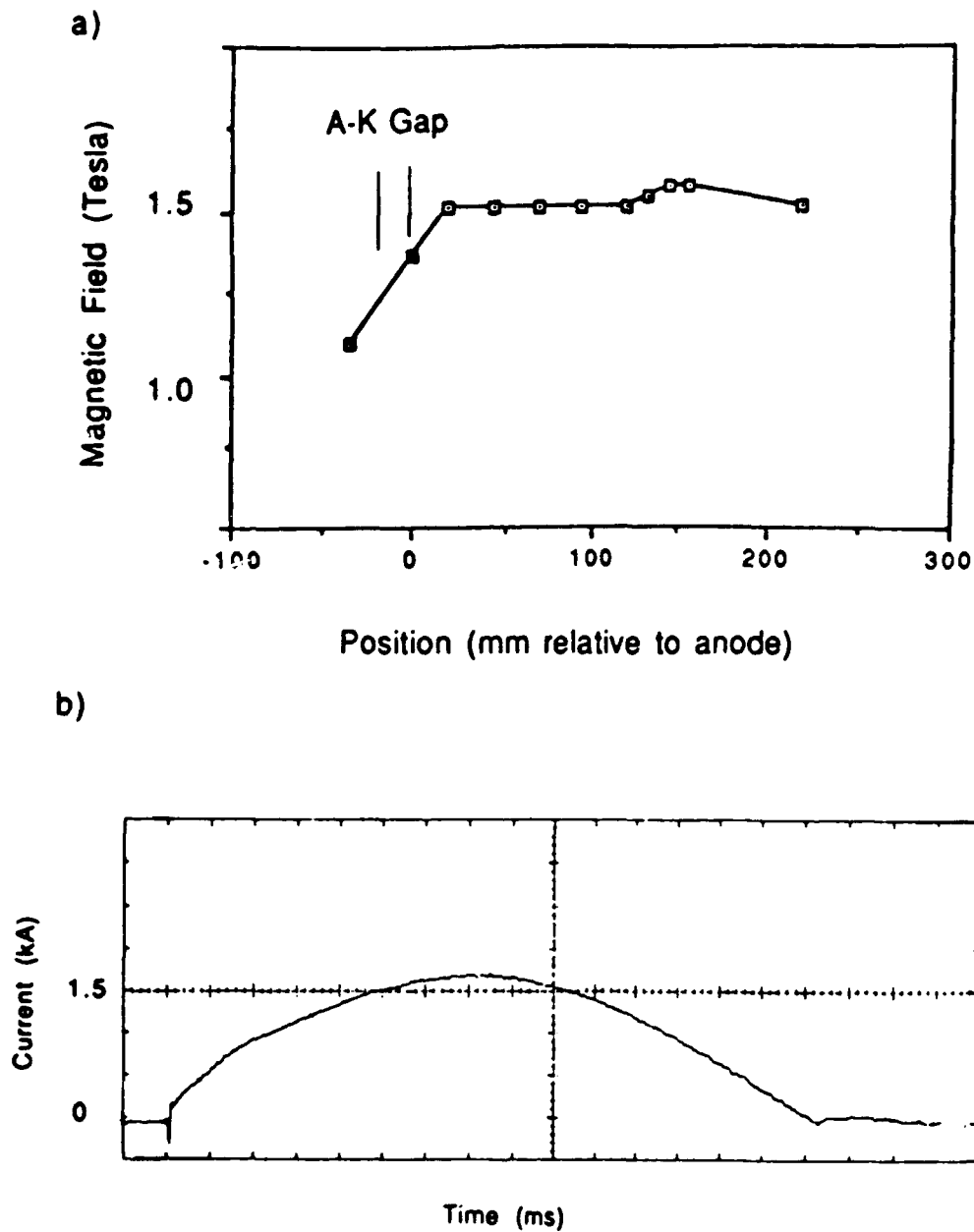_(Oscillogram of Current (kA) vs Time (ms))_

Time (ms)

FIG. 5. Experimentally measured profile of the magnetic field on axis: a) experimentally measured profile, and b) oscillogram of the current pulse powering the magnetic field coil at a capacitor charge of 6.0 kV.

about 7 ms. The coil circuit is sufficiently resistive that the ignitron shuts off after a half-cycle of the current pulse. The relatively long quarter-cycle rise of the current pulse ensures that the magnetic flux completely penetrates the metal hardware in the coil system.

In designing the magnetic field coil, two important considerations were:

i) the electron beam needs to be born in a region of straight magnetic flux lines to minimize beam rotation, and

ii) the electron beam has to follow the tapering flux lines at the downstream end of the system to reach the carbon-lined beam dump located in the conical horn antenna so as to not interfere with the microwave output and detection system.

With these factors in mind, it was decided to fabricate the magnet coil in-house. The inexpensive nature of the components and the relative ease of construction were the primary driving forces on this decision.

Before fabrication, the coil was designed using MSUPER,[3] an azimuthally symmetric magnetic-field calculating program. In the design, it was decided to begin the calculations on the aluminum vacuum flange that supports the Lucite insulating ring stack, which is located at a radial position $r = 8.5$ cm. A stainless steel tube with 8.5 cm radius, 0.3 cm wall thickness, and 30 cm length was used as a mandrel for the copper windings. Four layers of No. 10 magnet wire were wound around a thin-walled Lucite tube set around the mandrel. The layers were separated with 363 DMD (Dacron-Mylar-Dacron) to inhibit layer-to-layer electrical breakdown. The outer-most winding was covered with another Lucite tube and the annular section defined by the two Lucite tubes was potted in high-strength epoxy. Results from the MSUPER calculation incorporating all flux-excluding structures is shown in Fig. 6.

Slow-Wave Structures

A number of slow-wave structures are available for use in the UNM experiments. The slow-wave structures used are cylindrical waveguides with a wall radius r_w that is sinusoidally rippled about a mean radius r_0 so that

$$r_w(z) = r_0 + r_1 \sin h_0 z, \tag{1}$$

where r_1 is the ripple amplitude, h_0 is the wavenumber of the wall ripple period $2\pi/z_0$,

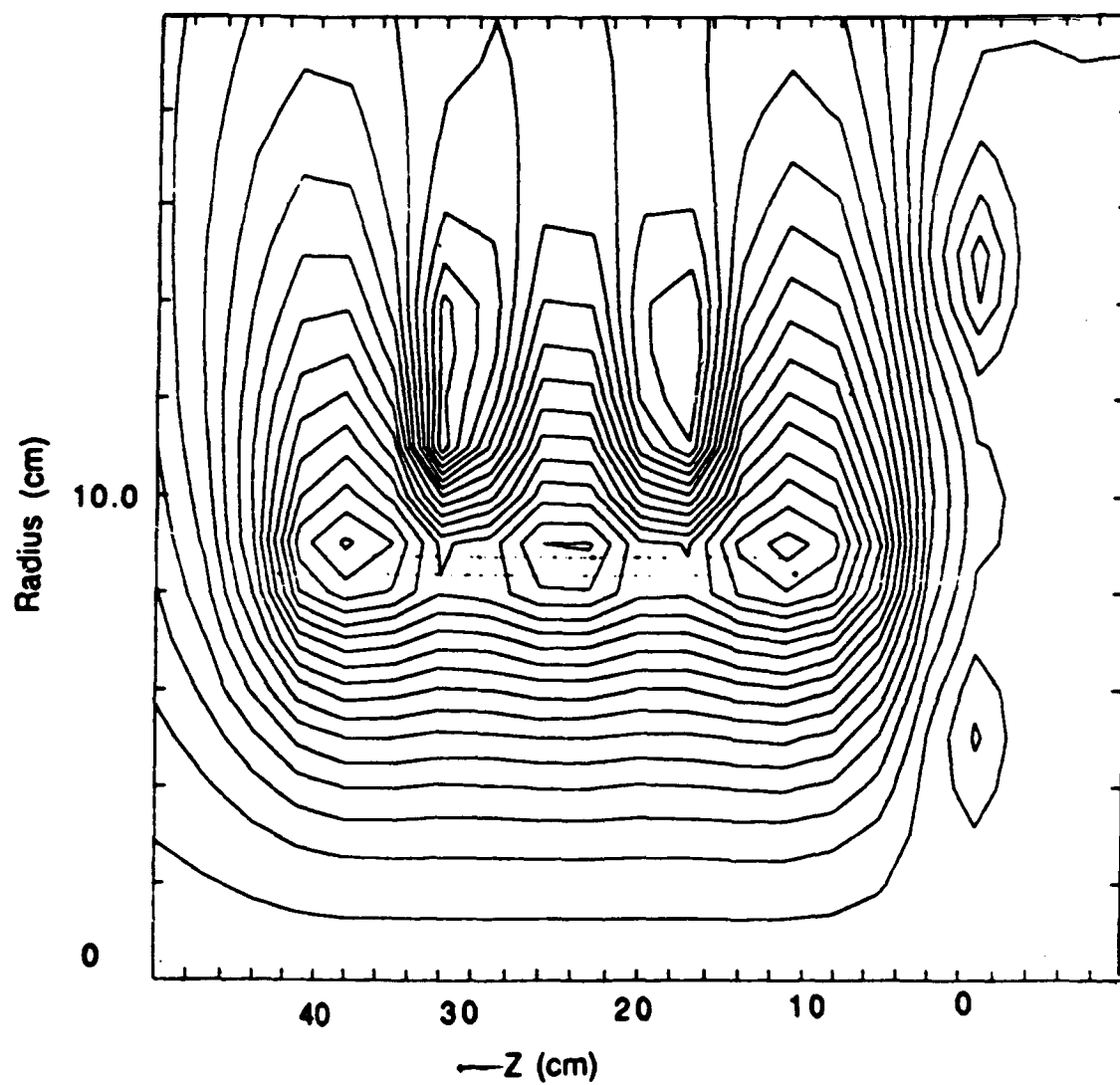FIG. 6. Magnetic field distribution in the $r - z$ plane calculated using MSUPER.
Two layers of copper winding are indicated at $r = 8 - 10$ cm.

and z_0 is the period of the wall ripple. For all the structures used, $z_0 = 1.1$ cm and $r_1 \ll r_0$. The parameters corresponding to the slow-wave structures used in the experiments are described in the table below.

TABLE I. Specific slow-wave structure parameters.

Struc. #	r_0 (cm)	r_1 (cm)
1	1.000	0.150
2	0.925	0.075
3	1.200	0.140

The effect of changes in the slow-wave structure parameters will be described in the next section of this final report.

III. Linear Theory of the UNM Short-Pulse BWO Interaction

Slow-Wave Interaction

The backward-wave oscillator is one form of a slow-wave device that converts the kinetic energy of an electron beam into microwave radiation. The structure derives its name from the fact that, because of the negative group velocity of the slow-wave structure mode at the beam resonance region, the energy transfer from the electrons to the electromagnetic modes has a Poynting vector lying antiparallel to the beam propagation velocity. The BWO consists essentially of an electron beam confined radially through a cylindrical resonant cavity containing some type of slow-wave structure. The slow-wave structure provides a set of periodically dispersive electromagnetic wave modes to the cavity with phase velocities parallel to the beam less than the speed of light.[4,5] When a relativistic electron beam is introduced into the slow-wave structure, an energy source is supplied which can produce an unstable interaction. This so-called "absolute instability"[6] is produced as the beam electrons interact throught the slow space charge wave with the transverse magnetic (TM) modes of the slow-wave structure. The TM modes have an axial electric field component which interacts with the negative energy space charge wave to decelerate and bunch the beam, transferring electron kinetic energy to the microwave radiation fields. The beam continues to be injected and, through positive reinforcement, the electromagnetic fields of the structure exponentially increase in amplitude at the frequency of the beam-structure resonance. The backward flowing rf power is reflected from the upstream end of the slow-wave structure and extracted along the direction of the electron beam.

A number of assumptions are made to analyze the electron beam in a smooth-walled-like cylinder:

1. the annular beam is infinitesimally thin and located at radius r_b, and carries a finite current I_b;

2. the guide magnetic field is infinite so that the beam's rotational velocity vanishes and the beam travels only in the $+z$ direction;

3. the waveguide wall is perfectly conducting and held at zero potential;

4. the waveguide is infinitely long and any observation point is far removed from the diode generating the beam so that the electric potentials in the waveguide depend only on the radial coordinate;

5. only TM_{0n} modes are considered.

Having made these assumptions, consider an annular beam with thickness much smaller than both the beam radius and the distance between the beam and the structure wall, propagating through a symmetric drift space with radius r_0. In this case, the electrostatic potential may be considered constant across the thin beam and the problem reduces to the solution of the homogeneous equation for the potential[7]

$$\frac{1}{r}\frac{d}{dr}\left(r\frac{d\phi}{dr}\right) = 0, \tag{2}$$

which is subject to the boundary condition

$$\phi(r = r_0) = 0, \tag{3}$$

and

$$\frac{d\phi}{dr}\Big|_{r \to r_b} = \frac{I_b}{2\pi\varepsilon_0 r_b v_b}, \tag{4}$$

where I_b is the beam current, and v_b is the longitudinal electron beam velocity (which is considered to be uniform across the beam).

From relativistic dynamics,

$$\gamma_b^2 = \frac{1}{1 - v_b^2/c^2}, \tag{5}$$

where c is the speed of light. For a relativistic electron beam, $\gamma_b > 1$. The solution for the potential distribution in the bounded system of infinite axial extent is[8]

$$\phi_r = \frac{I_b}{2\pi\varepsilon_0 v_b}\ln\frac{r_b}{r_0} \quad 0 \le r \le r_b \tag{6}$$

and

$$\phi_r = \frac{I_b}{2\pi\varepsilon_0 v_b}\ln\frac{r}{r_0} \quad 0 \le r \le r_b. \tag{7}$$

The cathode gamma is defined as

$$\gamma_c = 1 + \frac{|e\phi_c|}{mc^2}, \tag{8}$$

where ϕ_c is the potential impressed on the cathode, and $-e$ and m are the charge and mass of an electron, respectively.

The total injection energy at the cathode is

$$e\phi_c = (\gamma_c - 1)mc^2. \tag{9}$$

Similarly, the beam's kinetic energy is given as

$$e\phi_b = (\gamma_b - 1)mc^2. \tag{10}$$

From conservation of energy, we have that

$$e\phi_c = e\phi_b + \frac{eI_b}{2\pi\varepsilon_0 v_b} \ln\frac{r_0}{r_b}. \tag{11}$$

Solving for the beam current,

$$I_b = \frac{I_A(\gamma_b^2 - 1)^{1/2}}{2\ln(r_0/r_b)} \frac{\gamma_c - \gamma_b}{\gamma_b}, \tag{12}$$

where

$$I_A = \frac{4\pi\varepsilon_0 mc^3}{e} \simeq 17.1 \text{ kA} \tag{13}$$

is the Alfvén current. This equation has two possible solutions for beam kinetic energy as a function of beam current. The first corresponds to a high deceleration potential, which implies a lower steady state velocity and higher density. The second corresponds to a small deceleration velocity potential, which is related to particles of high velocity and low potential inside the drift space. The total energy in the system is less in the second case. The first state is therefore assumed unstable and the system prefers the second state.[9] From Eq. (12) it can be seen that $I_b = 0$ at $\gamma_b = 1.0$ and $\gamma_b = \gamma_c$. Figure 7 depicts Eq. (12) for various parameters. (The experiments described in Sec. IV of this report eventually utilized higher cathode potentials than depicted in Fig. 7.)

Consider a cylinder with $r_0 = 0.925$ cm. Figure 7(a) illustrates the dependence of beam current on γ_b with $r_b = 0.63$ cm, generated from a cathode with impressed potential ranging from $300 - 500$ kV. One can see that for $\gamma_b = 1.5$, I_b=1.5, 4.75,
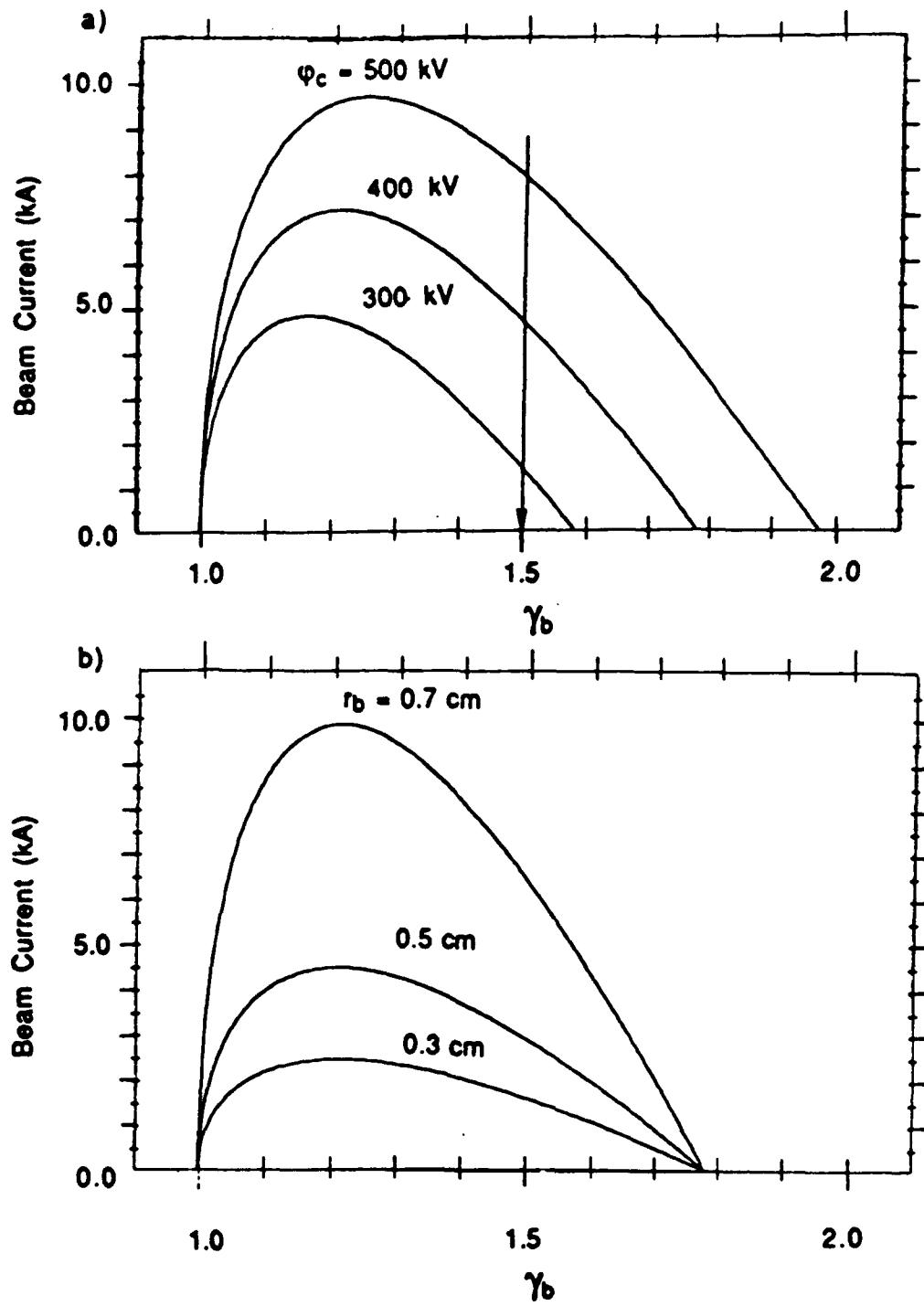
FIG. 7. Dependence of beam current on γ_b: a) $r_0 = 0.925$ cm, $r_b = 0.63$ cm, and $\phi_c = 300$, 400, and 500 kV; b) $r_0 = 0.925$ cm, $\phi_c = 400$ kV, and $r_b = 0.3$, 0.5, and 0.7 cm.

and 8.0 kA for each respective ϕ_c. For the case of an impressed potential of 400 kV, the injection energy is represented by $\gamma_c = 1.78$ and the beam, with $\gamma_b = 1.5$, has a reduction in gamma of 16% due to its space charge. Through Eq. (12) it is seen that if beam current is increased, the beam loses kinetic energy. This is the phenomenon of "space charge depression" and is important for two reasons. First, beam gamma affects the beam velocity which in turn affects the resonance with the modes of the slow-wave structure. Second, since a BWO converts the kinetic energy of an electron beam into microwave radiation, the overall efficiency of the device is reduced.

The peak of the curves in Fig. 7(b) represent the maximum current capable of propagating through the slow-wave structures for each parameter set. For any given geometry, the maximum is given at $\gamma_b = \gamma_c^{1/3}$, and Eq. (12) reduces to

$$I_{scl} = \frac{I_A(\gamma_c^{2/3} - 1)^{3/2}}{2\ln(r_0/r_b)} \tag{14}$$

which is the "space charge limited current."

If an electron beam is injected into a structure with a current that exceeds the space charge limiting current, then total transmission of the injected current is not possible. A virtual cathode forms and reflects some of the electrons back toward their injection point. This reflection creates a charge bunch which traps and reflects additional charge injected at later times. The charge bunch is similar to a single sheet of charge. The charge that was injected prior to the first reflection continues to cross the gap. As the charge exits the system, charges injected at later times are no longer trapped, but enter the system and form another single charged sheet. This continues until electrons can no longer enter the slow-wave structure.[10]

Waves on Beams

Space charge waves on an electron beam can be understood in terms of plasma oscillations in a drifting medium. A self-consistent derivation can be found elsewhere.[11] The dispersion relation for a relativistic beam is

$$(\omega - kv_b)^2 = \frac{n_b e^2}{\gamma_b^3 \epsilon_0 m}, \tag{15}$$

where n_b is the beam density. Note that the frequency is Doppler shifted by k times
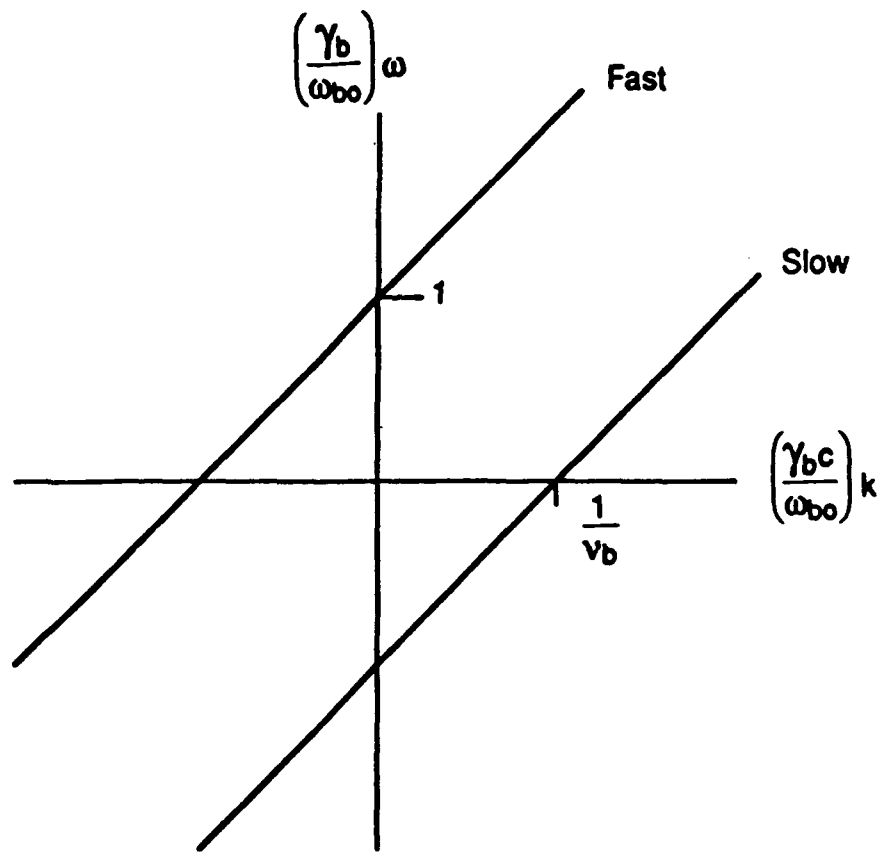
FIG. 8. Dispersion curve for a beam of relativistic electrons streaming through a stationary neutralizing background with velocity v_b.

the beam velocity; second, there is a relativistic factor γ_b^3 in the denominator on the right hand side. The dispersion relation may be written in terms of the relativistic plasma frequency

$$\omega_{b0}^2 = \frac{n_b e^2}{\gamma_b \varepsilon_0 m} \tag{16}$$

as

$$\omega_{b0}^2 = \gamma_b^2 (\omega - k v_b)^2, \tag{17}$$

or alternatively,

$$v_\phi = \frac{\omega v_b}{\omega \pm \omega_{b0}/\gamma_b}, \tag{18}$$

where v_ϕ is the phase velocity. This equation represents two straight lines, as indicated in Fig. 8. The group velocity is

$$v_g = \frac{\partial \omega}{\partial k} = v_b. \tag{19}$$

The phase velocity takes all values from $-\infty$ to ∞. For a given value of k, there exist two waves with phase velocities above and below the streaming velocity v_b. The solution with the negative sign is a wave with $v_\phi > v_b$ and is the fast space charge wave. If the phase velocity is greater than the drift velocity of the beam, then energy must be added to the system in order for it to be excited and microwave fields to grow. This is the positive energy mode.

The solution with a positive sign is a wave with $v_\phi < v_b$ and is the slow space charge wave. To excite and grow the microwave fields for this wave, the beam electrons must have velocities less than the electron beam instantaneous velocity. This is a negative energy mode and the wave must give up energy to develop. As the slow space charge wave is excited and the beam electrons are slowed down, excess energy is released into the microwave fields.

The frequency of operation for a BWO can be established by considering the resonances between the slow space charge waves and the cavity modes of the slow-wave structures. The Raman regime of operation is when the space charge waves become important. The slope of the slow space charge wave curves is dependent on the effective beam energy $e\phi_b$. The beam gamma may be changed by varying the beam injection energy $e\phi_c$ or by varying the beam current density, which affects the

space charge depression of the beam and is the mechanism responsible for pushing the slow space charge wave away from the beam line.

Full Dispersion Relation

To generate the dispersion curves for a beam/slow-wave structure interaction relevant to the experiments described in this report, Swegle's linearized fluid approach is utilized.[8] The periodicity of the structure permits each quantity associated with the TM waves to be expanded in a series according to Floquet's theorem,

$$E_z(r, z, t) = \sum_{n=-\infty}^{\infty} E_{zn}(r) \exp[i(k_n z - \omega t)], \tag{20}$$

where $k_n = k + n h_0$ and $-h_0/2 < k < h_0/2$. The wave equation for the axial component of electric field in cylindrical coordinates becomes

$$\frac{1}{r} \frac{d}{dr} \left(r \frac{dE_{zn}(r)}{dr} \right) + \Gamma_n^2 E_{zn}(r) = 0, \tag{21}$$

where $\Gamma_n^2 = \omega^2/c^2 - k_n^2$ and $r \neq r_b$. The solution so that E_{zn} is finite at the origin is

$$E_{zn} = A_n J_0(\Gamma_n r) \quad 0 \leq r \leq r_b \tag{22}$$

and

$$E_{zn} = B_n J_0(\Gamma_n r) + C_n Y_0(\Gamma_n r) \quad r_b \leq r \leq r_w, \tag{23}$$

where J_0 and Y_0 are the Bessel functions of the first and second kind, respectively, and A_n, B_n, and C_n are constants. To satisfy the continuity of the electric field and the requirement of a finite solution on the axis, the following equation for the tangential field at the wall must be satisfied:

$$E_t(r_w) = \sum_{n=-\infty}^{\infty} A_n \exp(inh_0 z) \left(1 + \frac{ik_n}{\Gamma_n^2} \frac{\partial}{\partial z} \right) \left(J_0(\Gamma_n r_w) - \alpha \left(\frac{\Gamma_n c}{\omega - k_n v_b} \right)^2 J_0(\Gamma_n r_w) \right.$$

$$\left. \times [J_0(\Gamma_n r_w) Y_0(\Gamma_n r_b) - J_0(\Gamma_n r_b) Y_0) \Gamma_n r_w)] \right) = 0, \tag{24}$$

where $\alpha = \pi I_b / \beta_b \gamma_b^3 I_A$ and $\beta_b = v_b/c$. Note that the cold dispersion relation results when $\alpha \to 0$.

Equation (24) is not an adequate solution since it contains z and the undefined coefficents A_n. This is eliminated by expanding the expression in a Fourier series over a period z_0. The resultant equation can be written as a homogeneous matrix equation

$$\mathbf{D} \cdot \mathbf{A} = 0 \approx \sum_{n=-\infty}^{\infty} A_n D_{mn}. \tag{25}$$

The matrix D_{mn} is given as

$$D_{mn} = \frac{\omega^2 - k_m k_n c^2}{\Gamma_n^2 c^2} \left(I_{mn}^j - \alpha \left(\frac{\Gamma_n c}{\omega - k_n v_b} \right)^2 \right.$$

$$\left. \times J_0(\Gamma_n r_b)[I_{mn}^j Y_0(\Gamma_n r_b) - I_{mn}^y J_0(\Gamma_n r_b)] \right). \tag{26}$$

A nontrivial solution to Eq. (25) requires that

$$\text{Det } [\mathbf{D}] = 0, \tag{27}$$

which results in the dispersion relation relating ω and k. A computer code called BWOPLT,[12] originally written by Swegle,[8] is used to generate dispersion relations by truncating $\mathbf{D}$ to a reasonable size in a 5×5 matrix. This is the linear analysis.

A cold dispersion relation for structure #1 (refer to Table I) is shown in Fig. 9(a). A beam dispersion relation ($\gamma_b = 1.5$ and $I_b = 1.5$ kA) for structure #1, along with the beam line, is indicated in Fig. 9(b). Two space charge wave curves can be seen fanning out from the origin, straddling the beam line. Near the intersection region, the fast space charge wave interacts with the structure wave in a stable interaction and the structure wave is converted into a space charge wave (seen increasing as k increases), and the space charge wave becomes the structure wave. At the intersection region, the structure wave and the slow space charge wave intersect and instability results. Within a narrow band of frequencies and wavenumbers, the waves merge, causing a complex conjugate pair of solutions ω which then split into the structure and space charge waves. All three waves are purely oscillatory with real ω, except in the narrow band where the complex conjugate solutions occur.[12] It can be seen in Fig. 9 that the pattern for the TM_{02} mode is similar to the pattern for the dominant
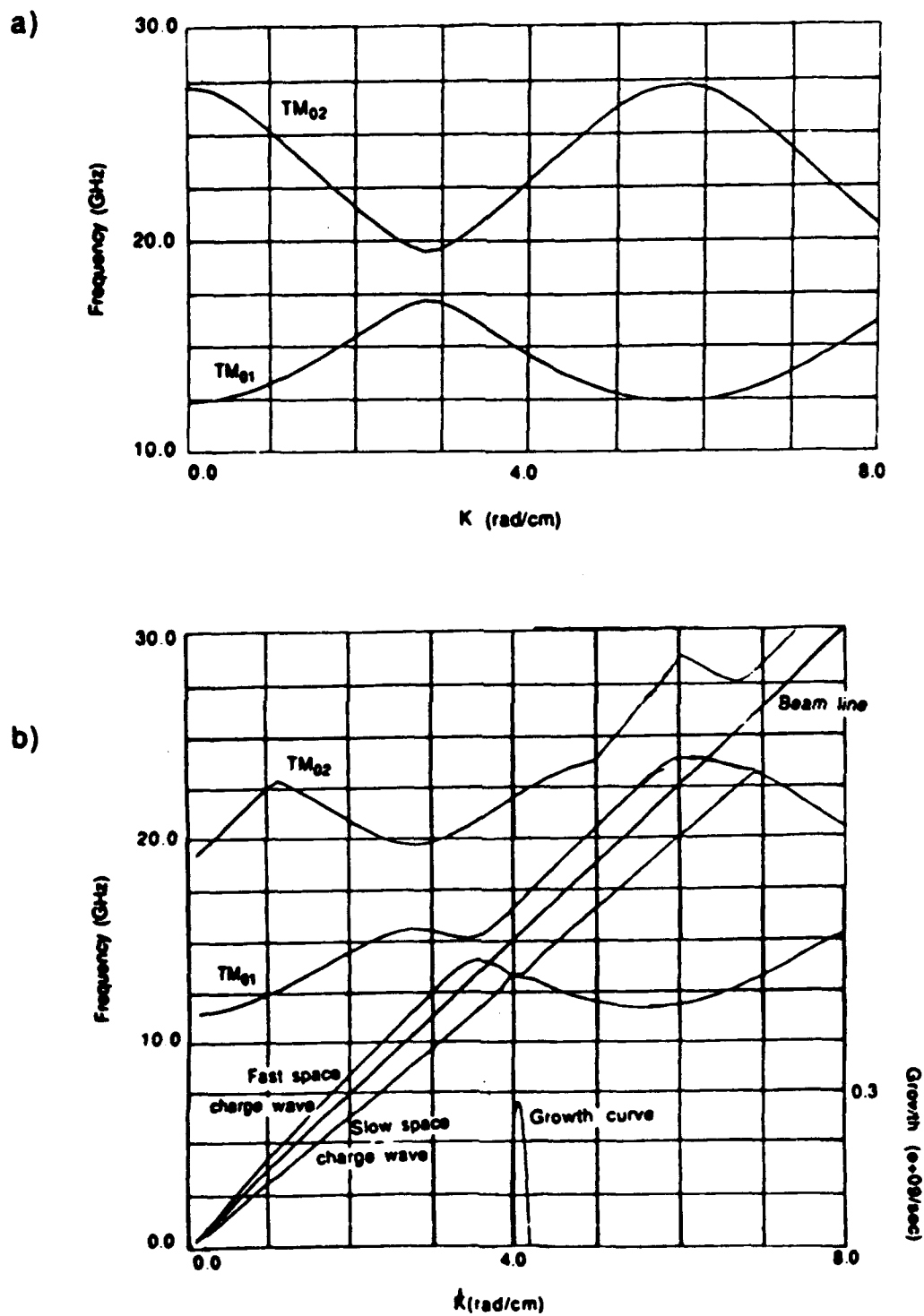
FIG. 9. Dispersion relation for slow-wave structure #1. a) cold dispersion relation, and b) beam dispersion relation.
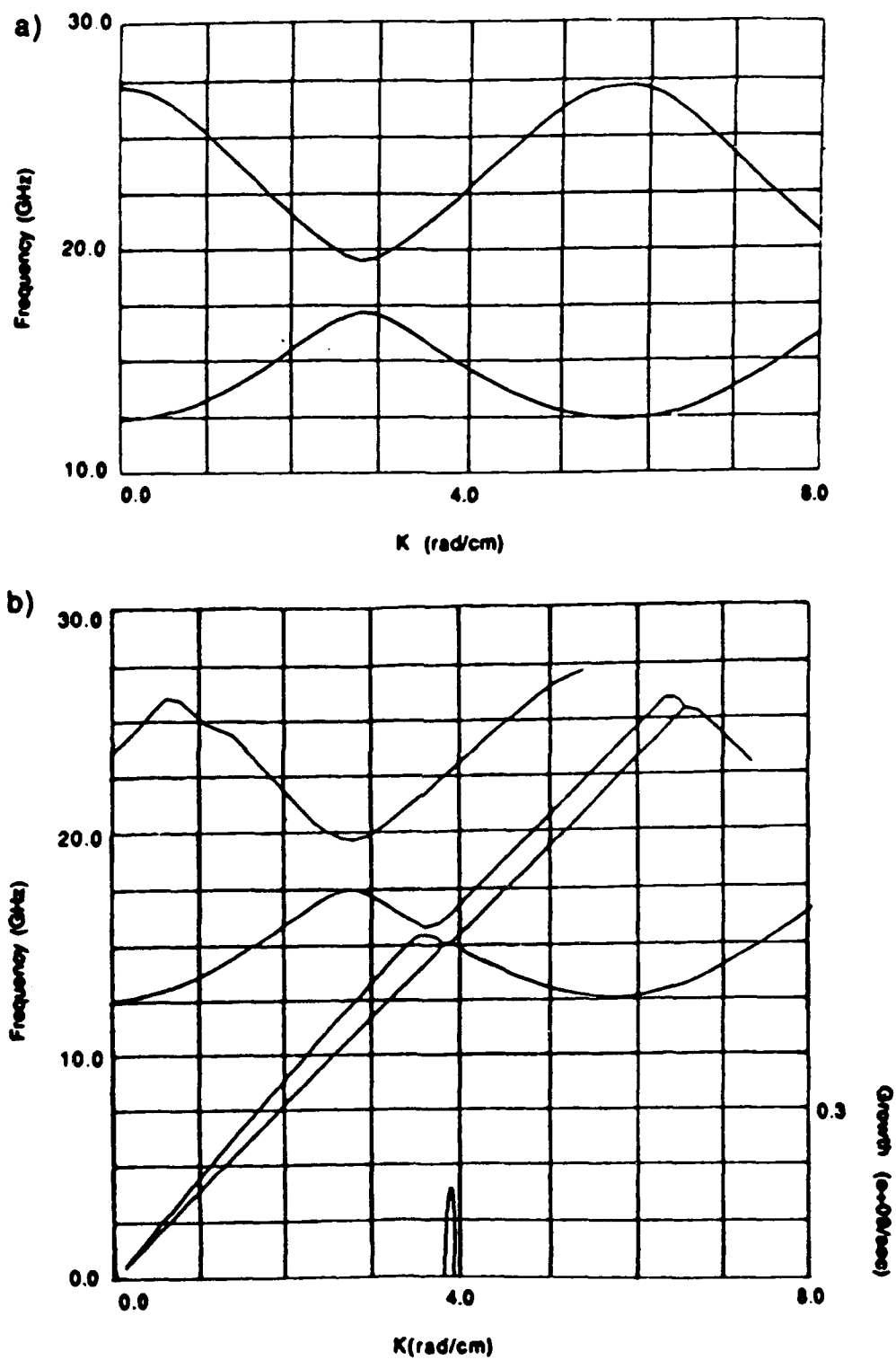
FIG. 10. Dispersion relation for slow-wave structure #2. a) cold dispersion relation, and b) beam dispersion relation.
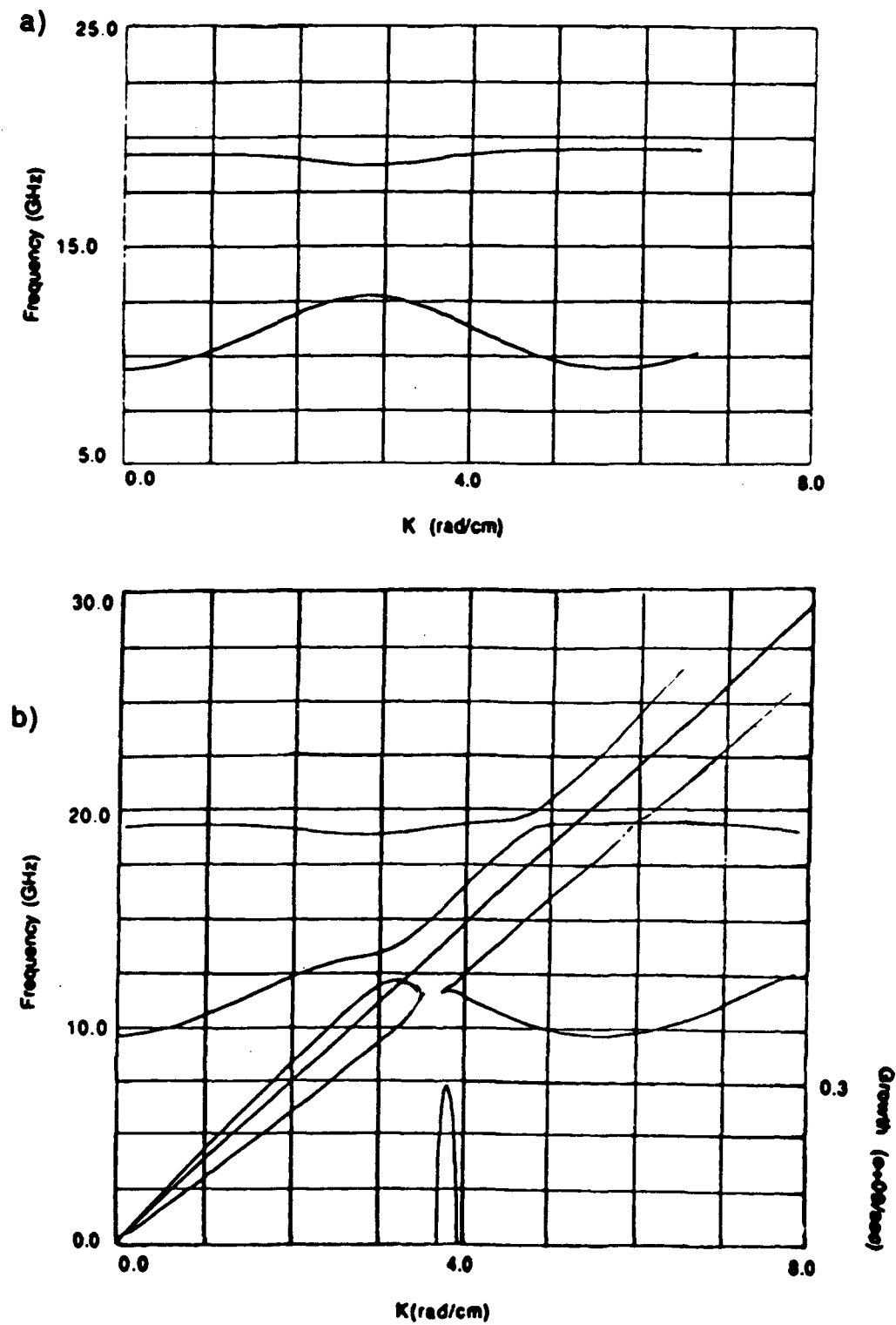
FIG. 11. Dispersion relation for slow-wave structure #3. a) cold dispersion relation, and b) beam dispersion relation.

mode. Similar results are obtained for structure #2 in Fig. 10 and structure #3 in Fig. 11.

Growth Rate

The BWO's growth rate is an assessment of the resonance frequency and the rate of increase of wave amplitude. This can be found by solving the dispersion relation for the beam–structure system for $\omega = (\omega_r + i\omega_i)$ *vs. k.*

The intersection of the slow space charge wave and the structure mode is tunable by varying the slope of the slow space charge wave. Figure 12(a) shows the effect of varying the beam injection energy $e\phi_c$. As the beam energy increases, the interaction region of the slow space charge wave with the structure wave is shifted up the dispersion curve, which increases the oscillation frequency. The tunable range is limited by the passband of the structure and the electron beam parameters. Another way of tuning the growth rate is to vary the beam's current density, as shown in Fig. 12(b). It is seen that the frequency is fairly stable with an increase in the growth amplitude as r_b/r_0 is increased. An enhanced interaction is expected as the beam moves outward toward the structure walls, since the space charge fields then become stronger. Figure 12 also shows the bandwidth expected with this structure. A BWO is known as a narrow bandwidth device, and this evident from the calculations.

The beam dispersion diagram for structure #1 (presented earlier) also shows the growth rate for the TM_{01} mode. The growth rate is approximately 0.27×10^9 s^{-1} at a frequency of 13.3 GHz. This growth rate will be compared with computational simulation results presented below.

Comparison with MAGIC Simulations

The operation of slow-wave structure #1 with the same electron beam parameters used in the BWOPLT analysis was also investigated using the 2-1/2 D fully electromagnetic particle-in-cell code MAGIC.[13] Figure 13 presents the development of the axial component of electric field in the system. The electric field is observed to grow exponentially until saturation. The dominant frequency of operation is determined to be approximately 14 GHz. The bottom portion of the figure illustrates the bunching of the beam. The linear BWOPLT calculations appear to be a good approximation to
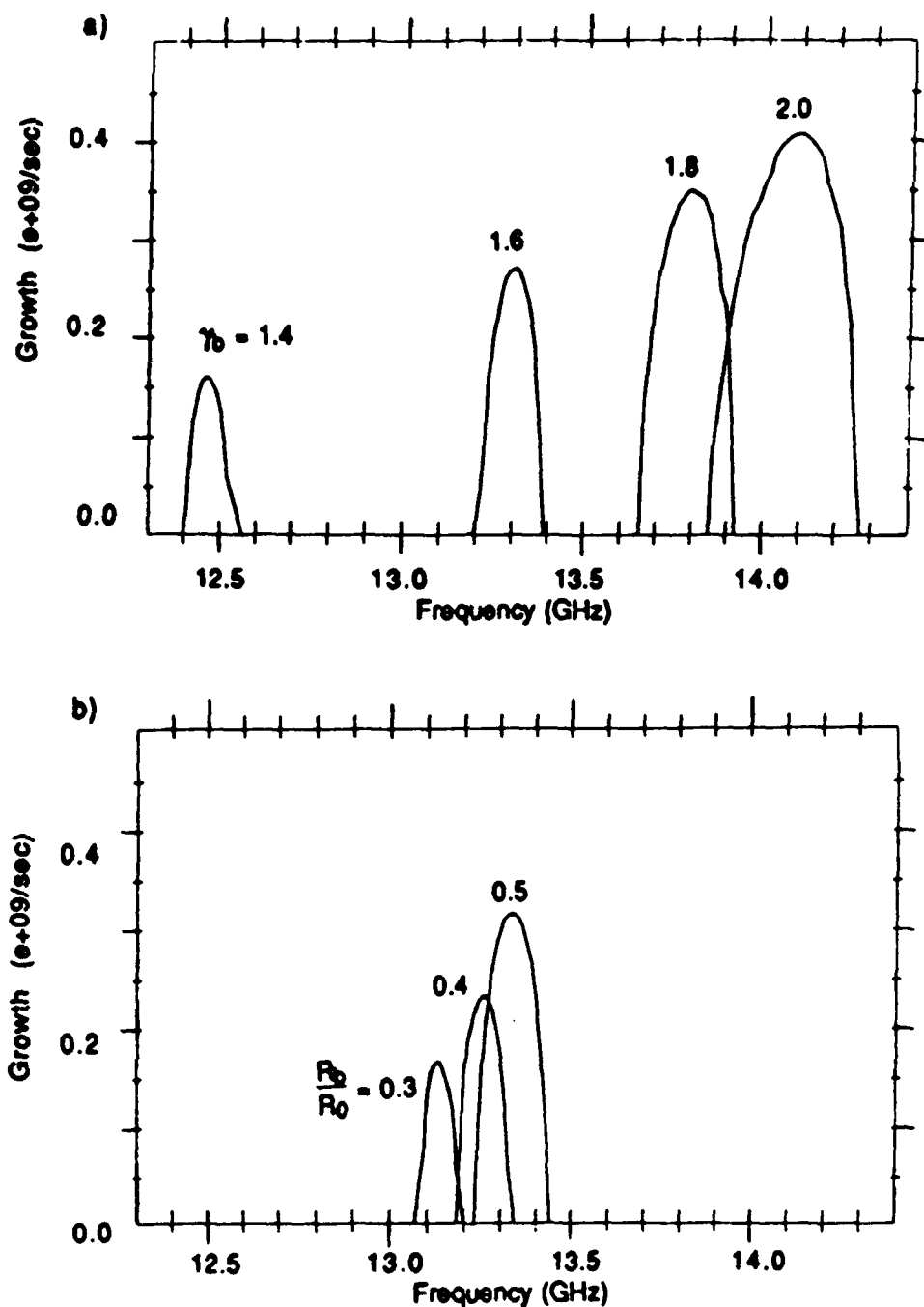
FIG. 12. Structure #1 growth rate: a) effect of varying the the beam injection energy, γ_b=1.4, 1.6, 1.8, and 2.0; b) effect of varying the beam current density through r_b/r_0=0.3, 0.4, and 0.5.
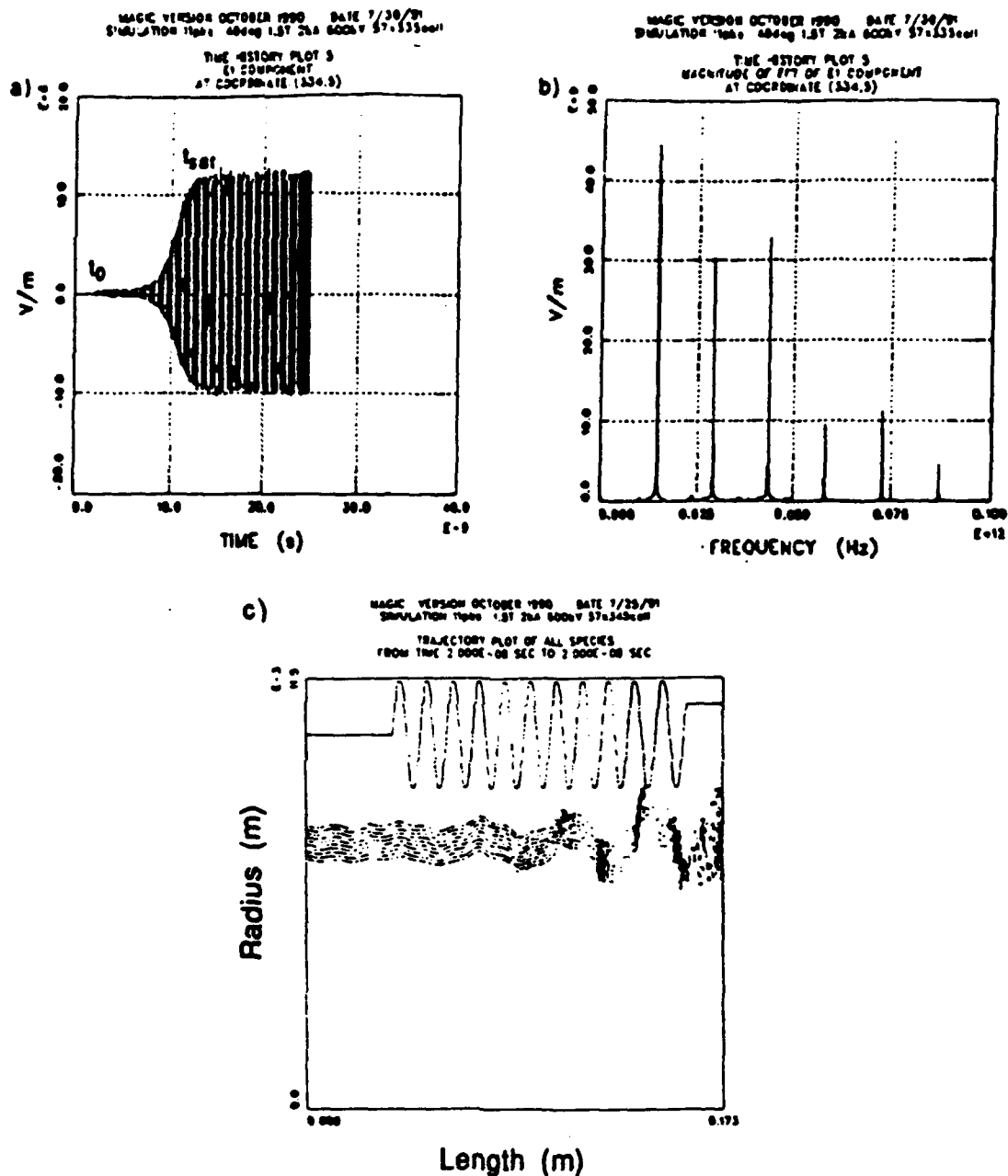
FIG. 13. MAGIC simulation of slow-wave structure #1. The axial electric field *vs.* time and a fast Fourier transform of the axial electric field are shown on top. A particle trajectory plot of electrons in the slow-wave structure is shown on the bottom.

the more complete MAGIC simulations. Differences between the two analyses may be attributed to finite length considerations which are neglected in the BWOPLT analysis. Additional MAGIC simulation results performed on a CRAY computer at Phillips Laboratory are presented in Appendix C of this report.

Conclusions from the Theoretical Studies

The results of the theoretical analyses presented in this section indicate that for a relativistic electron beam with cathode potential $\phi_c = 400$ kV and beam current $I_b = 1.5$ kA the UNM short-pulse BWO experiment should generate microwave radiation for each of the three slow-wave structures as noted in Table II:

TABLE II. Radiation frequency and growth rates.

Struc. #	ω_0 (GHz)	γ ($\times 10^9$) s^{-1}
1	13.30	0.2710
2	14.09	0.1560
3	11.75	0.2865

MAGIC predicts the growth rate for one run using structure #1 to be approximately 0.25×10^9 s^{-1}. The BWOPLT calculations were in close agreement with this value. It can be concluded that the 16 ns Nereus electron beam pulse width should be sufficient to excite the dominant BWO instability in the experiment. Based on operational efficiencies on the order of 5% observed by previous researchers using similar slow-wave structures,[14] the UNM short-pulse BWO can be expected to produce on the order of 10 MW of TM$_{01}$ microwaves at a frequency about 13-14 GHz.

An important consideration in these analyses is that the electron beam was assumed to be azimuthally symmetric. As will be seen in the next section, beam disruption and/or nonuniformity may dramatically alter the character of the beam–structure interaction, resulting in negligible generation of TM$_{01}$ radiation.

IV. Microwave Generation in the UNM Short-Pulse BWO Experiment

To preface this section, it should be stated that the entire data base has not yet been analyzed. The data set discussed in this section reflects the last series of experiments that was performed on the UNM short-pulse BWO experiment. A more complete discussion of the data and conclusions will be presented in a forthcoming M.S. thesis.[15]

Description of Data Base

The data set used in this section consists of Shots #913-1046. These can be broken down as follows (with the following notation: cathode radius=r_k, $A - K$ gap=d)

i) cathode parameters:

Shots 913-929: r_k=7.43 mm, d=6.75 mm

Shots 930-932: r_k=7.43 mm, d=6.00 mm

Shots 933-1046: r_k=7.43 mm, d=4.97 mm

ii) slow-wave structures (SWS):

Shots 913, 925-980, 1024-1037, 1045-1046: SWS#1

Shots 914-924: SWS#1 with smooth pipe (null test)

Shots 981-991: SWS#3

Shots 992-1008: SWS#2

Shots 1009-1023: SWS#3 with smooth pipe (null test)

Shots 1038–1044: Straight pipe with 7.5 mm radius (null test check).

The cathode voltage on many of these shots was 720 kV with an 8 ns pulse width (FWHM). A plot of beam current as a function of beam gamma for the updated voltage is presented in Fig. 14. The updated voltage is about 50% greater than the cathode potentials used in the calculations presented earlier. The capacitance in the Nereus/Blumlein circuit results in a voltage "ring-up" factor that was not taken into account in the early data sets. A uniform magnetic field with magnitude 0.7 T resulted in the largest measured microwave power. Three different slow-wave structures were used whose parameters correspond to the structures for which the
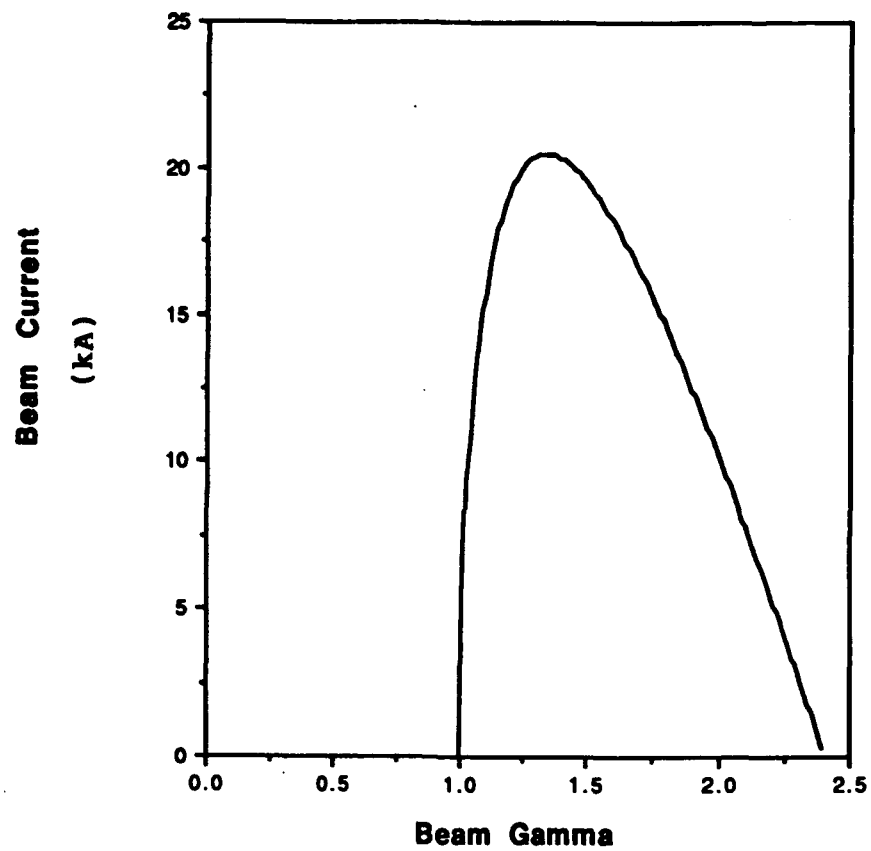
FIG. 14. Dependence of beam current I_b on beam gamma γ_b for an updated cathode potential $\phi_c = 720$ kV.

calculations were performed. A conical horn antenna was the output radiator. A section of its wall was lined with a copper-coated graphite insert which provided a low-Z beam dump to reduce *bremsstrahlung* x-rays. The thin copper film over the graphite provided a conducting surface to the microwave fields.

The conical horn antenna radiated into an *anechoic* chamber where another horn-antenna was located at various angular positions to measure the output radiation. This receiving antenna fed into a 100.6 m long dispersive delay line.[16] Power was measured at the input and output of the dispersive delay line. The dispersive delay line is comprised of Ku-band waveguide (WR-62 waveguide measuring 0.79 × 1.58 cm). The guide has a cutoff frequency of 9.49 GHz and the next highest mode appears at 18.75 GHz. The dispersive delay line was calibrated with sample waveforms, as illustrated in the top of Fig. 15. The time delay as a function of frequency for the delay line is given by

$$t = \frac{L}{c\sqrt{1-(f_c/f)^2}}, \tag{28}$$

where t is the transit time, L is the length of guide, and f_c is the cutoff frequency. The time delay as a function of frequency is presented in the bottom of Fig. 15. The uncertainty in the frequency discrimination Δf is given by

$$\Delta f = -\frac{f[(f/f_c)^2 - 1]}{t} \Delta t. \tag{29}$$

The uncertainty for the present configuration is less than 500 MHz.

Presentation of Data

The plot presented in Fig. 16 is FWHM beam current *vs.* FWHM cathode voltage for our data set. The data should fall along a straight line. The scatter in the data about a straight line is a measure of the general scatter in the data in the experiment.

By the time the experiments resulting in the data base under consideration were being conducted, the microwave and beam diagnostics were well-calibrated and reliable. The precision of the microwave frequency measurements enabled us to conclude that, at best, the BWO interaction was only a small part of the overall

CH1   DC   2mV /div   NORMAL   100nSEC/div
CH2   DC   5mV /div   NORMAL   100nSEC/div
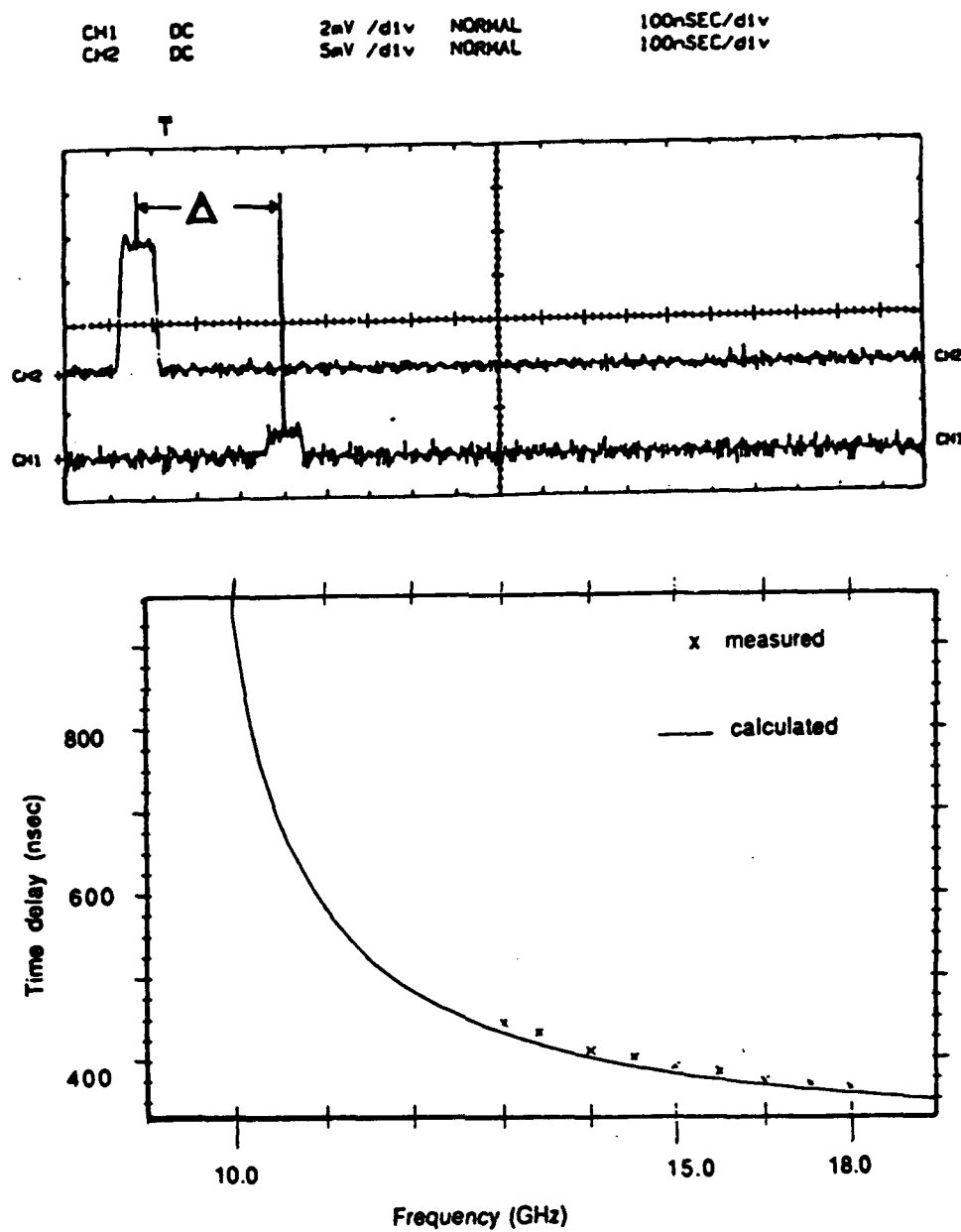
FIG. 15.   A sample calibration waveform for the dispersive delay line (top). Time delay *vs.* calculated and measured frequency for the Ku-band dispersive delay line (bottom).
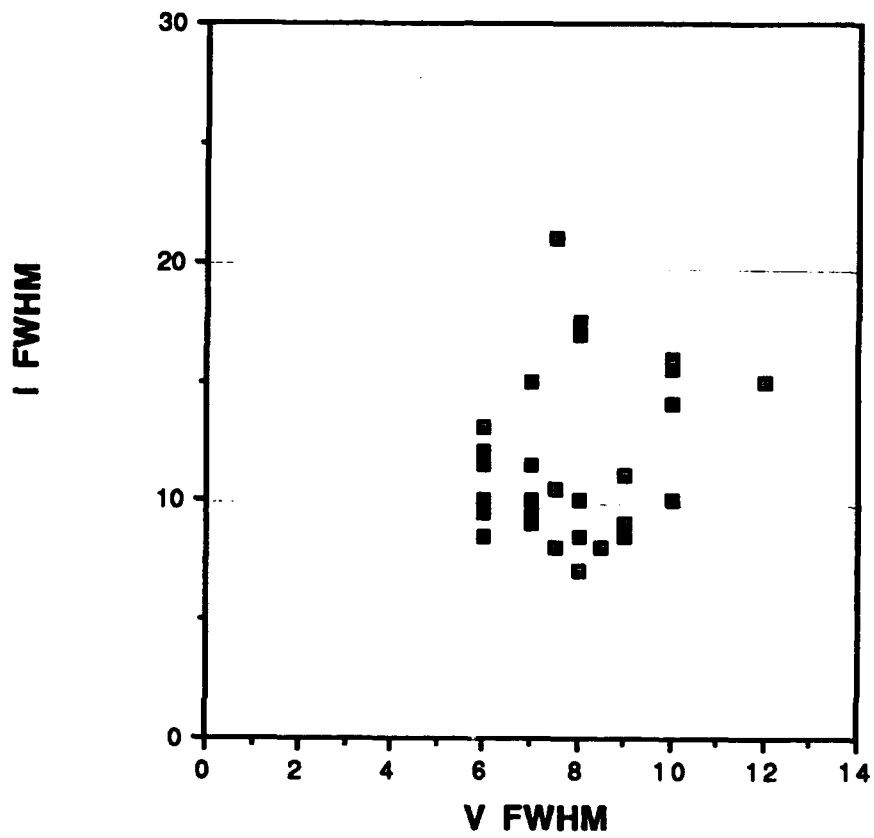
FIG. 16. Plot of FWHM beam current *vs.* FWHM cathode voltage.

beam–structure interaction that was being observed. Previous frequency meaurements utilizing low-pass and high-pass filters[17] allowed us to conclude that the data were consistent with Ku-band microwave generation. However, the dispersive delay line proved that the frequency components were widely scattered and not simply due to dominant mode BWO interaction. In fact, the parameterizations led us to conclude that other factors were playing an important role in inhibiting the BWO interaction.

As an example of the anomalous dependence of microwave power generation, consider the plot of relative microwave power as a function of guide magnetic field, as indicated in Fig. 17. Previous researchers observed a general increase in microwave power as a function of guide magnetic field, except for a power dip at the magnetic field value corresponding to the relativistic cyclotron resonance.[18] In the experiments reported here, the peak generated powers corresponded to a field value of about 0.7 T and then gradually diminished at higher fields—no "double-humped" dependence was observed. At lower values of the guide field, the microwave power completely disappeared.

The most important measurement that can confirm BWO operation would be the dependence of the output microwave frequency on slow-wave structure and beam parameters. Consider the dependence of output frequency on γ_b for slow-wave structures #1-3. (These measurements were performed at an axial distance $z = 40$ cm away from the conical horn antenna at an angle 15° away from the axis.) The first comparison that will be done is the output frequency for each slow-wave structure at a given γ_b. Based on the analyses presented in Sec. III of this report, TM_{01} operation for the three structures would result in microwave output ranging from about 11-14 GHz. Since that analysis was performed for lower energy beams, one should scale these numbers a little higher. However, the higher γ_b corresponding to the updated cathode potential cannot account for the very high frequencies measured in the experiment. In fact, if anything, these high frequencies may be suggestive of TM_{02} operation. In addition, based on the earlier analyses, the frequency output should increase for a given set of beam parameters as one went from slow-wave structure #3-1-2. Careful consideration of Fig. 18 confirms that there is a general trend where SWS#3 values are consistently at a lower frequency than SWS#1 values. (There

Microwave Production is a Function of Magnetic Field
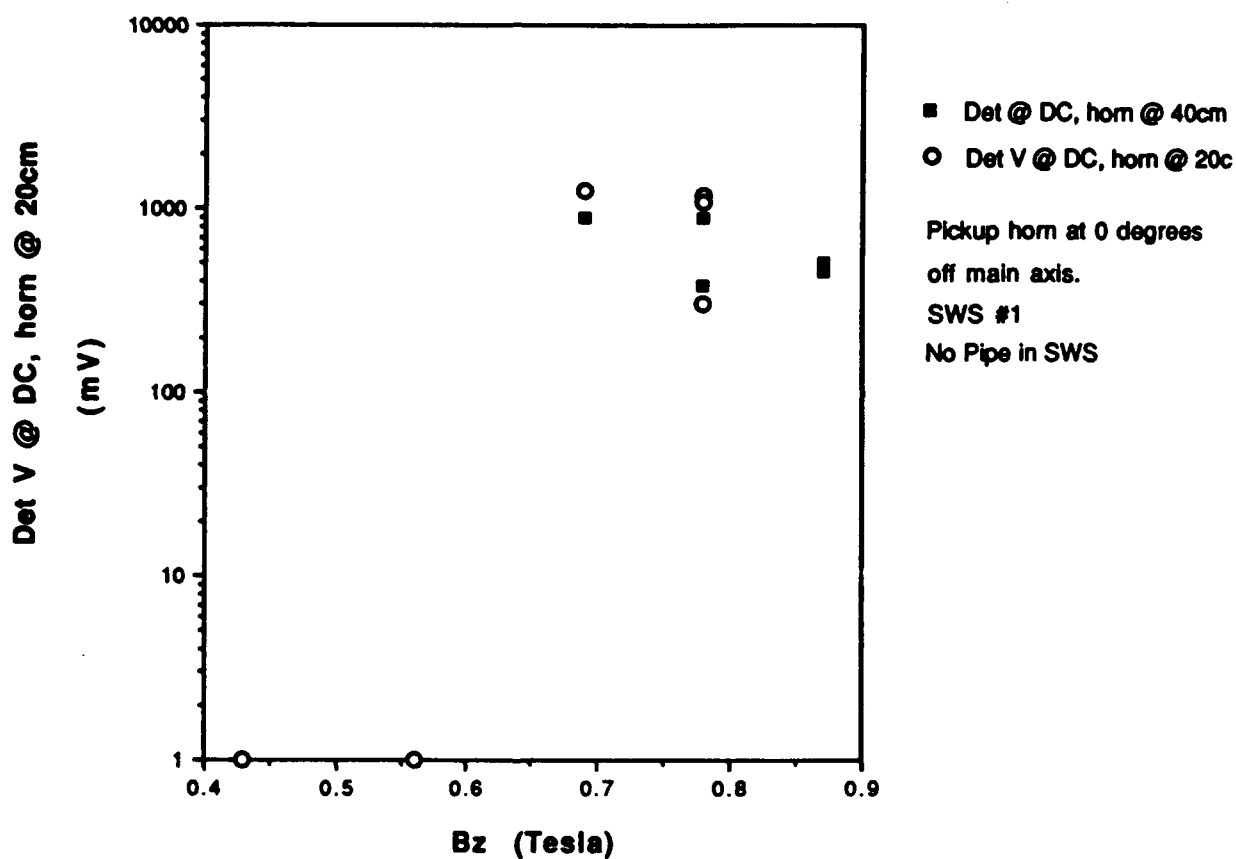
FIG. 17.   Dependence of relative microwave output power as a function of guide magnetic field.
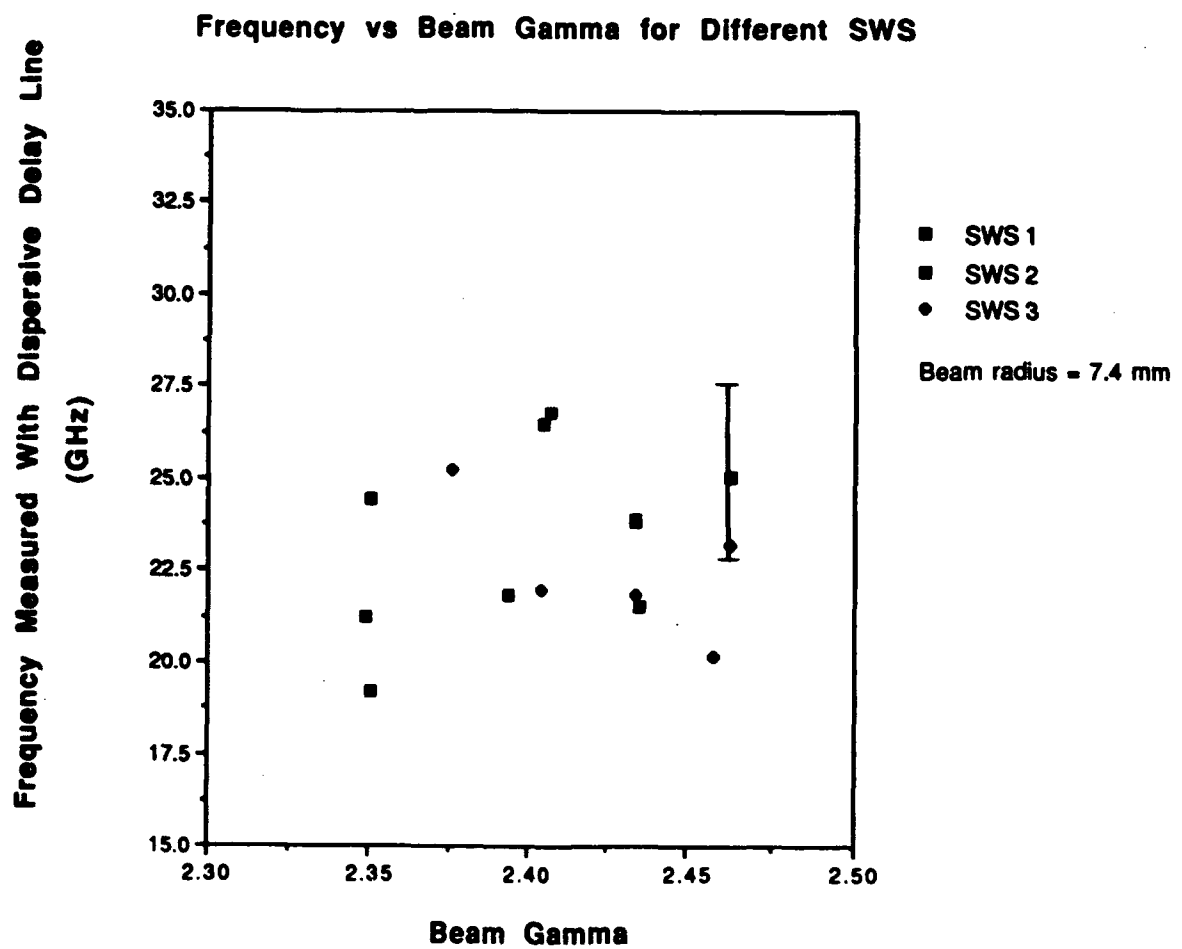
FIG. 18.   Plot of output microwave frequency as a function of γ_b for slow-wave structures #1-3.

was only one data point for SWS#2 so it was not used in this comparison.)

Butler, *et al.*[9] observed that the oscillation frequency of the BWO increases with increasing γ_b, eventually plateauing after a *critical* value. This cannot be confirmed in our data set, possibly because of the limited variation in γ_b, and because of the higher frequency mode of operation—their measurement was performed for dominant mode operation.

Another measurement that can confirm BWO operation is the dependence of output microwave frequency on beam current density. The linear analysis presented earlier indicated that frequency should increase slightly with increasing beam current (see Fig. 12(b) and Eq. (12) in this report) for constant cathode potentials. Figure 19 indicates that as the peak beam current increases, the trend is for increasing output microwave frequency for a given slow-wave structure. This is consistent with BWO operation at TM_{02}.

Before considering additional data, Fig. 20 plots the variation of vacuum base pressure measured before a shot as a function of shot number. This graph is important because it allows us to discard inconsistent data points which correspond to shots with high base pressure (bad vacuum).

Next is plotted the dependence of the relative microwave power output as a function of γ_b. Butler, *et al.*[9] observed that the relative output power of the BWO increases slightly with increasing γ_b, eventually plateauing after a *critical* value. (In actuality, the data points in their plots varied considerably about the plateau.) The data we present in Fig. 21 on the other hand indicates a general decrease in output power as a function of γ_b. This may be attributed to the fact that TM_{02} operation is observed and/or the presence of other mechanisms for the generation of the observed microwave radiation. The data points scattered along the abscissa correspond to the shots taken at high vacuum base pressures, as indicated in Fig. 20.

An important indication of microwave output is the distribution of a field component as a function of angle away from the axis of the conical horn antenna. This measurement not only indicates the mode of operation, but also allows one to estimate a total radiated power level. Initial experiments performed on the UNM short-pulse BWO device[17] verified microwave output in the radiating near-field region by viewing the electrical breakdown of an array of fluorescent light bulbs. This crude diagnostic
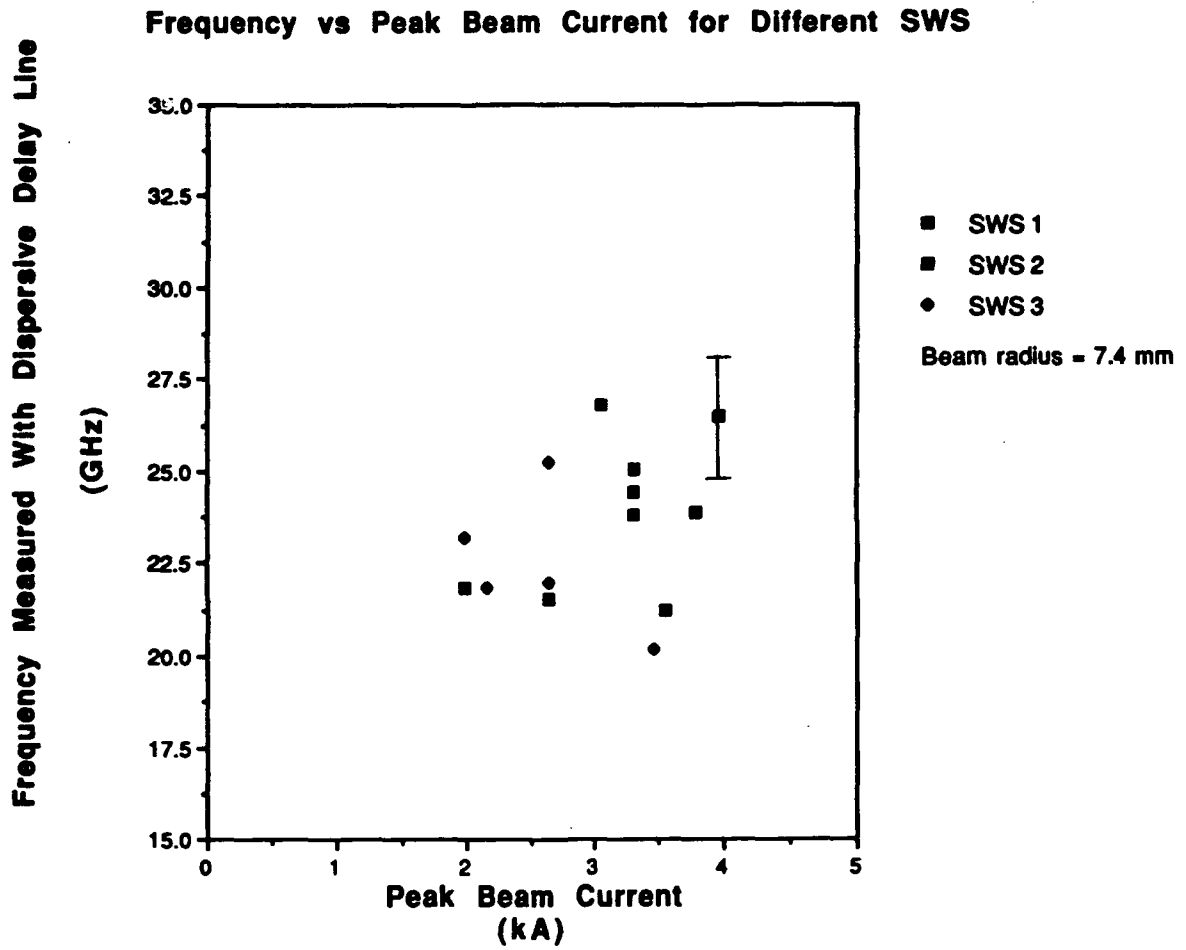
FIG. 19. Plot of output microwave frequency as a function of peak I_b for slow-wave structures #1-3.
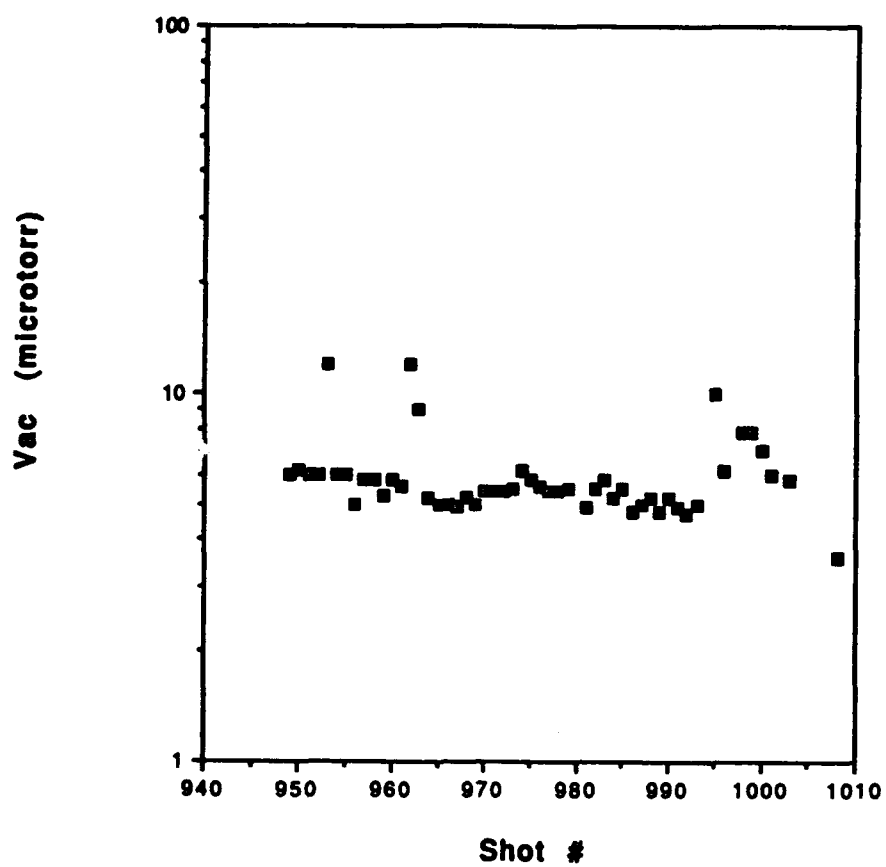
FIG. 20. Plot of vacuum base pressure as a function of shot number for our data set.

Output Power Is A Function Of Beam Gamma
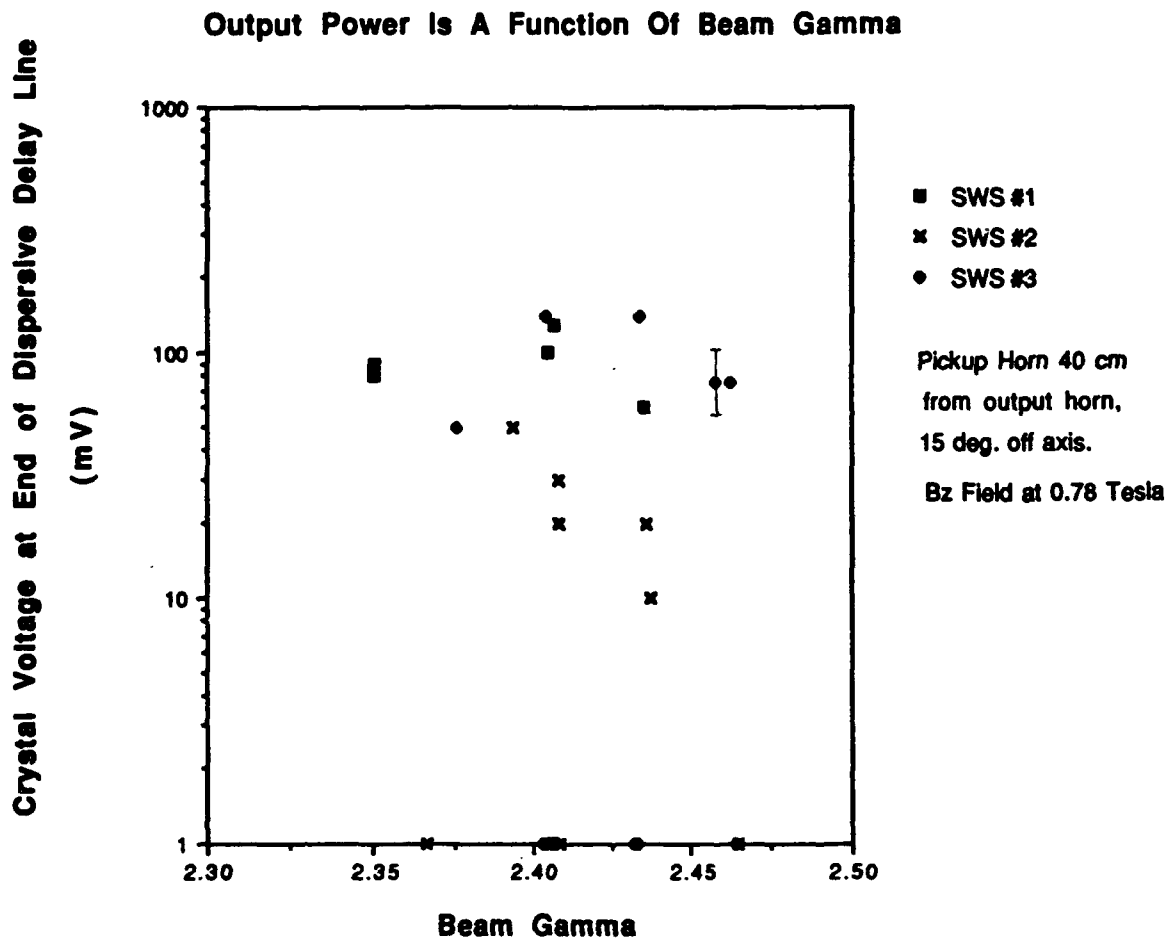
FIG. 21. Plot of relative output power as a function of γ_b for slow-wave structures #1-3.
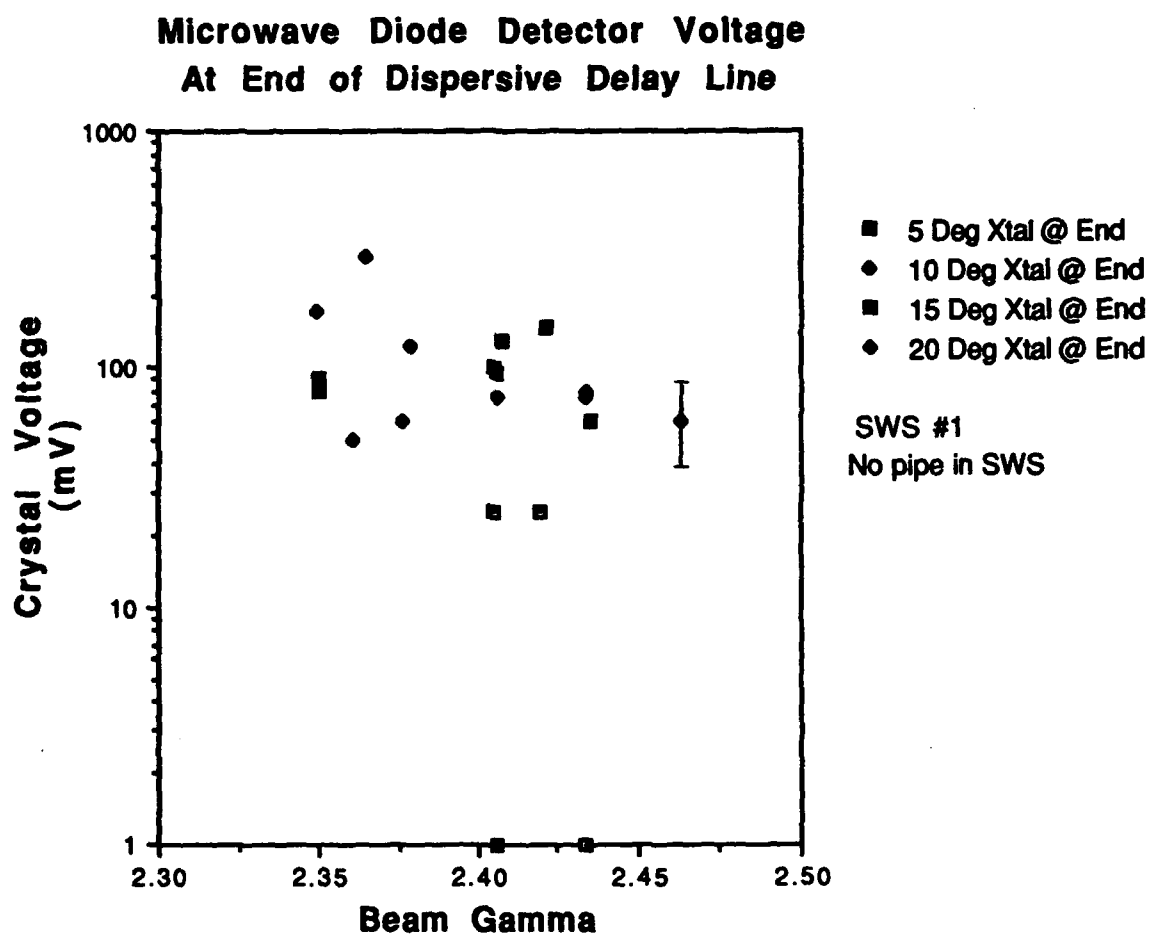
FIG. 22. Plot of relative output microwave power as a function of γ_b for slow-wave structure #1, measured at various angles off from the main axis of the antenna radiator.

Microwave Diode Detector Voltage
At End of Dispersive Delay Line
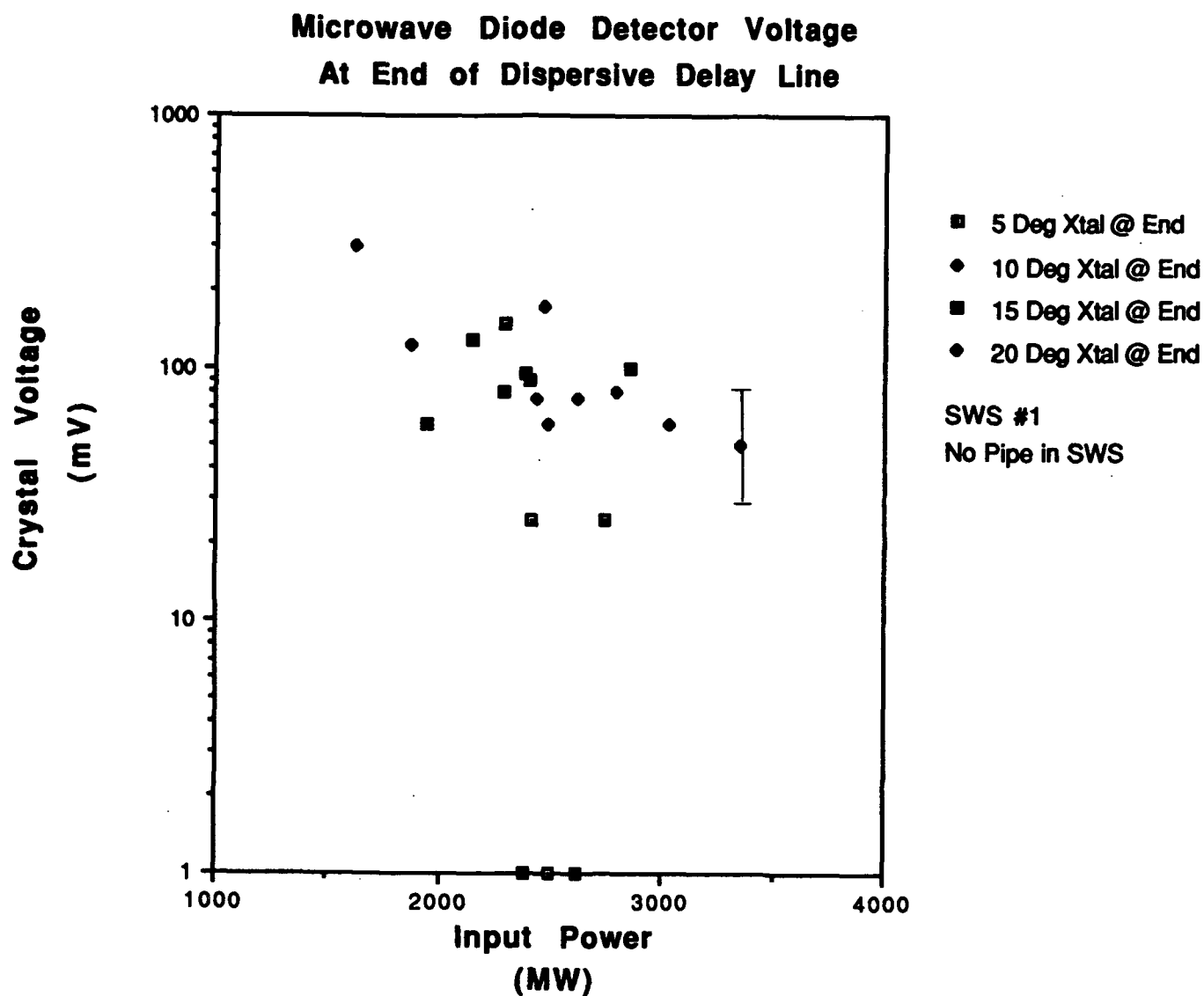
FIG. 23. Plot of relative output microwave power as a function of beam power for slow-wave structure #1, measured at various angles off from the main axis of the antenna radiator.

merely verified the presence of microwave electric fields and could not resolve any distinct mode pattern. Subsequent experiments described in this report utilized a horn antenna as a receiver that was mounted on a jig to allow measurements to be performed at any angle off the main axis of the radiating antenna, 40 cm into the *anechoic* chamber. Results from these measurements are summarized in Figs. 22 and 23. Important features from this plot are i) there is a general trend of decreasing microwave power with increasing γ_b and increasing beam power (consistent with the data plotted in Fig. 21), and ii) at a given value of γ_b or input beam power, the output microwave power is relatively uniform as you probe regions away from the axis of the radiator. This implies that there is some TE_{11}-like radiation pattern in addition to any TM_{02} radiation pattern.

Figure 24 presents a calculation of the distribution of H_ϕ and the total radiated power in the radiating near-field as a function of angle away from the axis. The calculation was performed using the program TM_{0n}.[19] The distributions in the figure were calculated for the TM_{01} mode, although calculations were performed for TM_{02} as well. The absence of the field null on axis in the measurements is consistent with the experiment not operating in the dominant mode. The application of the TM_{02} calculations to the relative powers measured in the UNM short-pulse BWO indicates that 0.01-0.1 MW of microwave power can be attributed to the BWO interaction.

H-phi 0.4 m from horn mouth
Calculated Using TMON Fields Program

05-15-1991   00017

LEGEND:
H-phi

NOTES: (00017)
Origin at Horn mouth
Probe 0.40 m from
  horn mouth
Freq = 13.6 GHz
Input power to horn
  1 MW in TM01 mode

Angle (degrees)

Total power 0.4 m from horn mouth
Calculated Using TMON Fields Program

05-15-1991   00014

LEGEND:
Total Power

NOTES: (00016)
Origin at Horn mouth
Probe 0.40 m from
  horn mouth
Freq = 13.6 GHz
Input power to horn
  1 MW in TM01 mode

Watts/cm^2

Angle (degrees)

FIG. 24. H_ϕ component of microwave field and total power as a function of angle, 40 cm downstream from the mouth of the conical horn antenna.

V. Additional Experimental Tasks Performed

In addition to the main experimental activities described in the previous section, two additional task were performed in parallel.

PI-110A Long-pulse Upgrade

The UNM Pulsed Power and Plasma Science Laboratory received a PI-110A Pulserad electron beam accelerator from Sandia National Laboratories. Part of our funding during this grant period was to upgrade this machine from a short-pulse, high voltage machine to a long-pulse, lower voltage machine for long-pulse BWO studies next year. To do this, the Blumlein transmission line was removed and a Type-A pulse-forming network (PFN) was constructed. The design for the upgrade was provided expense-free by Physics International Company[20] and basically involved adding an *LC*-filter to the output of the Marx generator. This upgrade was done several years ago for Dr. Lavern Schlee at the Air Force Weapons Laboratory for electron beam laser pumping applications. Subsequent discussions with Dr. Schlee[21] forced us to conclude that the original design was flawed since it allowed the capacitors in the PFN to exceed their voltage reversal limits. We proceeded to redesign the network and concluded that the inclusion of higher-voltage capacitors in the PFN should be adequate.

The PI-110A upgrade has been completed and the machine is ready to be operated. This machine will be used in the next grant period for long-pulse BWO studies at electron beam and slow-wave structure parameters identical to the short-pulse experiments described in this report. The only difference will be that the FWHM voltage pulse duration will be about 450 ns instead of about 8 – 16 ns, as indicated in Fig. 25.

Vlasov Antenna

During the past year Dr. Kyle Hendricks, a visiting scientist with our laboratory for two months, worked at the Air Force Phillips Laboratory with a radiator called a Vlasov Antenna.[22] The original Vlasov antenna design was modified by a group at Harry Diamond Laboratories into a device called a Shaped End Radiator (SER).[23]
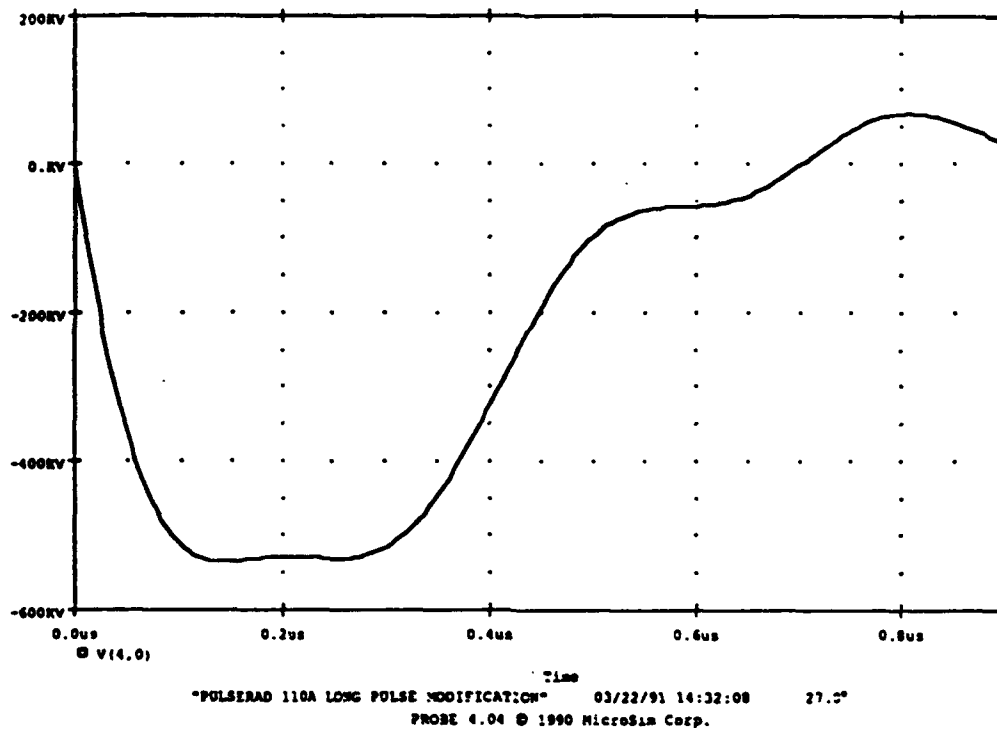
FIG. 25. Calculated voltage output of the upgraded PI-110A electron beam accelerator.

Basically, one takes a cylindrical smooth-walled waveguide and makes a bevel cut at an angle to the z-axis. Conceptually, one may view this antenna as taking one half of the annular TM_{01} pattern and folding it back onto the other half. The result is a "TE_{11}-like" pattern in the far-field.

This antenna would provide several benefits to the UNM-BWO experiments, provided that the power densities are below levels causing air breakdown. The primary benefits will be measuring total radiated power from a TE_{11} pattern and using the radiation output in applications. The power in this pattern is focused into a much smaller solid angle than that of a TM_{01} pattern. In addition, there is a high degree of linear polarization. As a result of cold test work done at Phillips Laboratory, the two orthogonal linear polarizations have been measured to differ by 10 dB.

Several antennas have been designed and constructed at the Phillips Laboratory for eventual use in the UNM experiments. Because of the higher order mode operation of the UNM short-pulse BWO, experiments with the Vlasov antenna have not been performed. It is anticipated that experiments will be performed in the next grant period using the long-pulse machine.

VI. Preliminary Conclusions

It is clear that the UNM short-pulse BWO experiment is not operating in the dominant TM_{01} mode as predicted by the linear theory and the MAGIC simulations. This conclusion is based on both the frequency measurements using the three different slow-wave structures and on the angular distribution of the radiated field amplitudes in the radiating near-field of the conical horn antenna. At the moment, we have two main explanations for this result:

---

1. the electron beam is disrupted as it propagates through the slow-wave structures

2. the diode voltage pulse is triangular so that predicted resonance occurs for a brief moment and there is a large spread in beam energy.

The disruption of the electron beam was studied by propagating the beam through slow-wave structures and straight pipes and measuring the azimuthal distribution of the electrons at various points along the direction of propagation. Witness plate diagnostics have indicated the break-up of the beam upon propagating 20 cm, as is evident in Fig. 26 (a) and (b). A calculation of the dispersion relation for the diocotron instability[24] using relativistic dynamics is presently being performed for the beam and structure parameters being used in the UNM short-pulse BWO experiment. Initial results indicate narrow stability regions in k-space (Fig. 26 (c)). The dispersion relation utilized was derived in Ref. 25. Various cathode configurations, including both thin-walled and thicker-walled emitters, were used in the experiments to isolate the BWO generation of microwaves from the radiation produced by beam break-up effects. These shots were the so-called "null tests" indicated in the data base. The apparent competition between the BWO interaction generating TM mode radiation and beam disruption generating TE-like modes was observed previously in experiments in the former Soviet Union.[26]

Finally, we believe that the azimuthal asymmetry observed in the electron beam is due to a disruption as opposed to nonuniform cathode emission due to a "screening effect"[27] since the beam asymmetry was observed to "evolve" as it propagated. We
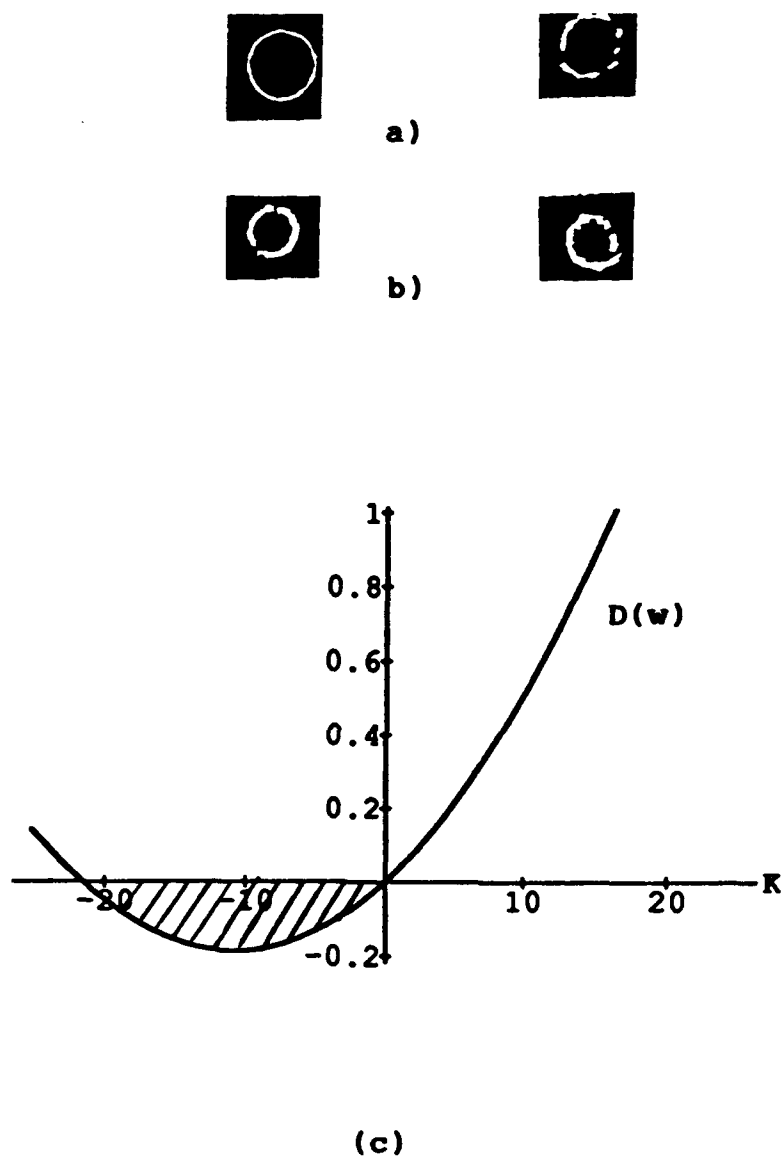
FIG. 26. Witness plate diagnostic of electron beam profiles. (a) Effect of changing wall radius on beam distribution, and (b) effect of magnetic field on beam distribution. (c) Plot of the dispersion relation for the diocotron instability for the experimental parameters. The shaded region represents a narrow region of stability to high-l mode perturbations.

believe that the beam break-up may be caused by a design flaw in the short-pulse BWO experiment which allowed for a large radial cathode-to-ground spacing in the $A - K$ gap region of the field-immersed diode. Our design appears to contradict earlier designs (see for example the discussion in Ref. 18). This is being studied in detail and results will be presented in a forthcoming thesis.[15]

The effects of a triangular voltage pulse distribution may also be interrupting the BWO interaction. This was suggested by Dr. Baruch Levush.[28] His recent studies indicate that the electron beam pulse shape may be critical in determining the efficiency of the BWO interaction. This point is presently being investigated for the UNM short-pulse BWO parameters. The fact that previous experiments in the former Soviet Union[18] utilizing short time duration, triangularly-shaped pulses were very successful will allow for interesting comparison with both the UNM short-pulse BWO data and the nonlinear BWO theory.

VII. Future Plans

Our experience with short-pulse BWO generation will now be useful in researching repetitively-pulsed high-power BWO operation. The UNM Pulsed Power and Plasma Science Laboratory is expecting the delivery of a SINUS-VI repetitively-pulsed electron beam accelerator with an X-band BWO front end (Fig. 27) in May, 1992. This device utilizes a 500-600 kV, 1-5 kA electron beam, generated at a 200 Hz repetition rate, to radiate over 500 MW of 3 cm radiation in 12 ns pulse durations. This device, which operates at a remarkable 20% efficiency, will clearly enable our group to learn the physics of these microwave generating devices from experts in the world.

Additional tasks for the new grant period will be researching new materials for incorporation in high-power microwave tube devices, new electron sources for repetitively-pulsed electron beam accelerators, and effects of plasma-fill on long pulse BWO devices.
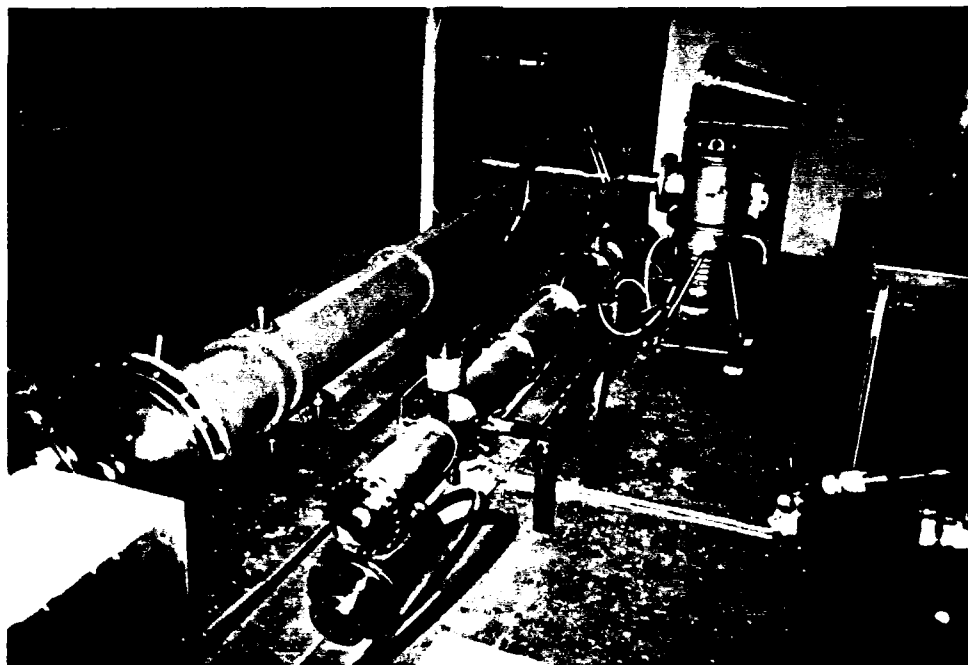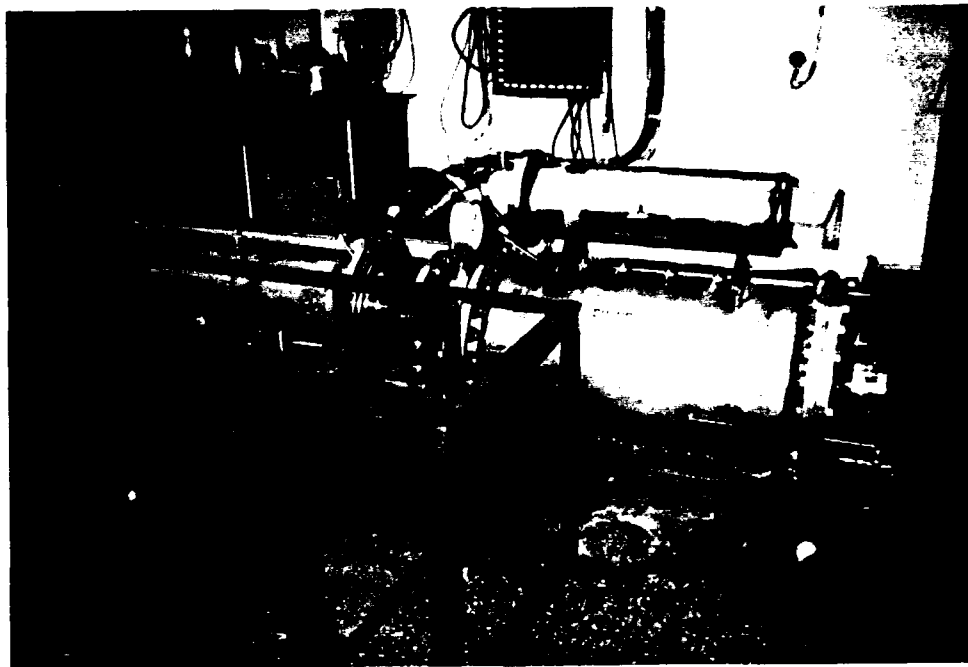
FIG. 27. Photographs of a SINUS-VI repetitively-pulsed electron beam accelerator being constructed for the UNM BWO g. up at the High Current Electronics Institute, Siberian Academy of Sciences, Tomsk, Russia.

VIII. References

1. R. S. Clark, "Nereus Marx Generator, a 600 Kilovolt–1.5 KiloJoule Unit," Sandia National Laboratories Development Report SC-DR-71 0216 (1971).

2. S. Humphries, Jr., *Principles of Charged Particle Acceleration* (John Wiley & Sons, New York, 1986), p. 250.

3. L. R. Miller, computer code MSUPER (available on blackstone.eece.unm.edu, 1990).

4. A. H. W. Beck, *Space-Charge Waves and Electromagnetic Waves* (Pergamon Press, New York, 1958).

5. J. R. Pierce, *Traveling-Wave Tubes* (D. Van Nostrand, New York, 1950).

6. J. D. Lawson, *The Physics of Charged-Particle Beams*, 2nd Ed. (Clarendon Press, Oxford, England, 1988), p. 337.

7. W. H. Louisell, *Coupled Mode and Parametric Electronics* (John Wiley & Sons, New York, 1960).

8. J. A. Swegle, J. W. Poukey, and G. T. Leifeste, Phys. Fluids **28**, 2882 (1985).

9. J. M. Butler, C. B. Wharton, and S. Furukawa, IEEE Trans. Plasma Sci. **18**, 490 (1990).

10. R. B. Miller, *An Introduction to the Physics of Intense Charged Particle Beams* (Plenum Press, New York, 1982).

11. J. D. Lawson, *The Physics of Charged-Particle Beams*, 2nd Ed. (Clarendon Press, Oxford, England, 1988), p. 293.

12. Computer code BWOPLT (available on blackstone.eece.unm.edu, 1990).

13. B. Goplen, R. E. Clark, J. McDonald, and W. M. Bollen, *Users' Manual for MAGIC/Version-Oct. 1990*, Mission Research Corporation Technical Report MRC/WDC-R-246 (1990). Simulations performed at the Air Force Phillips Laboratory by L. Bowers.

14. G. T. Leifeste, L. M. Earley, J. A. Swegle, J. W. Poukey, R. B. Miller, C. E. Crist, C. B. Wharton, and W. P. Ballard, J. Appl. Phys. **59**, 1366 (1986).

15. J. Bradley, *Measurement of Microwave Generation in the UNM Short-Pulse Backward-Wave Oscillator*, University of New Mexico M.S. Thesis (in preparation).

16. J. A. Nation, Rev. Sci. Instrum. **41**, 1097 (1970).

17. E. Schamiloglu, J. M. Gahl, J. Bradley, and G. McCarthy, "Ku-Band Radiationin the UNM Backward-Wave Oscillator Experiment," SPIE **1407** *Intense Microwave and Particle Beams II*, p. 242 (1991).

18. V. L. Bratman, G. G. Denisov, M. M. Ofitserov, S. D. Korovin, S. D. Polevin, and V. V. Rostov, IEEE Trans. Plasma Sci. **15**, 2 (1987); S. D. Korovin (private communication, 1991).

19. Computer code TM_{0n}, E. Baca (private communication, 1991).

20. B. Bernstein (private communication, 1990).

21. L. Schlee (private communication, 1990).

22. S. N. Vlasov and I. M. Orlova, "Quasioptical Transformer which Transforms the Waves in a Waveguide Having a Circular Cross Section into a Highly Directional Wave Beam," Radiofizika **17**, 148 (1974).

23. B. G. Ruth, R. K. Dahlstrom, C. D. Schlesinger, and L. F. Libelo, "Design and Low-Power Testing of a Microwave Vlasov Mode Converter," *1989 IEEE MTT-S International Microwave Symposium Digest"* III, p. 1277.

24. See, for example, R. C. Davidson, *Physics of Nonneutral Plasmas* (Addison-Wesley, Redwood City, CA, 1990), Chap. 6.

25. C. A. Kapetanakos, D. A. Hammer, C. D. Striffler, and R. C. Davidson, Phys. Rev. Lett. **30**, 1303 (1973).

26. V. S. Ivanov, S. J. Krementsov, V. A. Kutsenko, M. D. Raizer, A. A. Rukhadze, and A. V. Fedotov, Sov. Phys. Tech. Phys. **26**, 580 (1981).

27. G. A. Mesyats and D. I. Proskurovsky, *Pulsed Electrical Discharge in Vacuum* (Springer-Verlag, Berlin, 1989), p. 175.

28. B. Levush, T. M. Antonsen, Jr., A. Bromborsky, W. R. Lou, and Y. Carmel, "Theory of Relativistic Backward-Wave Oscillators with End Reflections," IEEE Trans. Plasma Sci. (in press); B. Levush (private communication, 1991).

Appendix A. GRA's and Visiting Scientists

Graduate Research Assistants

Two graduate students have participated on the UNM-BWO project over the last two years. Gary McCarthy recently defended his M.S. thesis and Joe Bradley will be defending his thesis in the Spring 1992 semester.

1. G. McCarthy, *Calculation of the Operational Characteristics of the UNM Short-Pulse Backward-Wave Oscillator*, University of New Mexico M.S. Thesis (December 1991).

2. J. Bradley, *Measurement of Microwave Generation in the UNM Short-Pulse Backward-Wave Oscillator*, University of New Mexico M.S. Thesis (in preparation). This thesis will be submitted as a supplement to the final report upon completion.

Visiting Scientists

Two visiting scientists have participated in the UNM-BWO project over the last grant period.

1. Dr. K. C. Mittal, whose permanent title is Scientific Officer, Plasma Physics Division, B.A.R.C., Bombay, India, came to work with us in the summer of 1991. He was a visiting research scientist with the Laboratory of Plasma Studies, Cornell University, and came to the University of New Mexico through a mutual agreement with the Cornell group. Dr. Mittal participated on the high-current, electron beam transport studies.

2. Dr. Kyle Hendricks, who is now permanently affiliated with the Air Force Phillips Laboratory, worked in conjunction with us for about two months. His prime task was to develop a Vlasov antenna radiator for use in the UNM experiments. An antenna was prepared by Dr. Hendricks, but was not used during the grant period since the short-pulse BWO experiment did not operate reliably in the dominant TM_{01} mode. The radiator that Dr. Hendricks developed will be used on the long-pulse BWO experiment to come on line during the new grant period.

Appendix B. Conference Presentations and Seminars Presented

One conference paper and two conference poster sessions were presented during the grant period:

1. E. Schamiloglu, J. M. Gahl, J. Bradley, and G. McCarthy, "Ku-Band Radiationin the UNM Backward-Wave Oscillator Experiment," SPIE 1407 *Intense Microwave and Particle Beams II*, p. 242 (1991).

2. J. Bradley, G. McCarthy, J. Gahl, and E. Schamiloglu, "Measurement of Ku-Band Radiation Generated in the UNM Backward-Wave Oscillator," Proceedings of the 1991 IEEE International Conference on Plasma Science (Williamsburg, VA, 1991), p. 128.

3. J. Bradley, G. McCarthy, K. C. Mittal, P. W. Werner, J. Gahl, C. Fleddermann, and E. Schamiloglu, "Experiments on Alternate Beam Transport Techniques in a Backward-Wave Oscillator," Bull. Am. Phys. Soc. **36**, 2424 (1991).

In addition, Professor Schamiloglu gave seminars on the UNM Short-Pulse BWO Experiment at:

1. Electrical Engineering Department, University of Texas at El Paso (April 19, 1991)

2. High Current Electronics Insitute, Siberian Academy of Sciences, Tomsk, Russia (October 21, 1991).

Appendix C. Additional MAGIC Simulation Results

The attached simulation results were performed by researchers at Phillips Laboratory in conjunction with the UNM BWO group. The parameters studied are indicated.

PARAMETER STUDY

1.	BEAM CURRENT	1	2	8	kA
2.	INNER BEAM RADIUS	4.6	5.6	6.6	mm
3.	BEAM ANNULAS THICKNESS	1	2		mm
4.	SINUSOID PERIODS	8	9	10	

SIMULATION: 8pke 75deg 3.7 1kA 600kV 7l=310
TRAJECTORY PLOT OF ALL SPECIES
FROM TIME 1.912E-08 SEC TO 1.913E-08 SEC

SIMULATION: 8pke 75deg 3.7 2kA 600kV 7l=310
TRAJECTORY PLOT OF ALL SPECIES
FROM TIME 1.912E-08 SEC TO 1.913E-08 SEC

SIMULATION: 8pke 75deg 3.7 8kA 600kV 7l=310
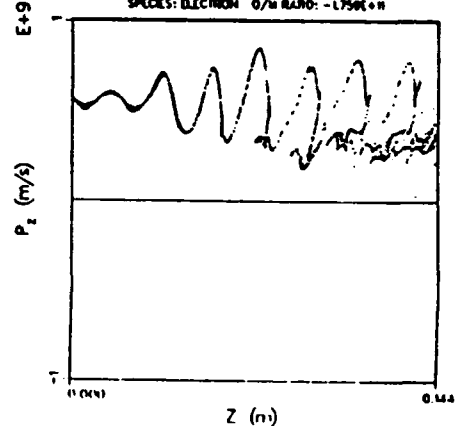TRAJECTORY PLOT OF ALL SPECIES
FROM TIME 1.912E-08 SEC TO 1.913E-08 SEC

SIMULATION: 8pke 75deg 3.7 1kA 600kV 7l=310
PHASE-SPACE PLOT OF PZ VS. Z AT TIME: 1.91E-08 SEC
SPECIES: ELECTRON Q/M RATIO: -1.750E+11

SIMULATION: 8pke 75deg 3.7 2kA 600kV 7l=310
PHASE-SPACE PLOT OF PZ VS. Z AT TIME: 1.91E-08 SEC
SPECIES: ELECTRON Q/M RATIO: -1.750E+11

SIMULATION: 8pke 75deg 3.7 8kA 600kV 7l=310
PHASE-SPACE PLOT OF PZ VS. Z AT TIME: 1.91E-08 SEC
SPECIES: ELECTRON Q/M RATIO: -1.750E+11

Z (m)

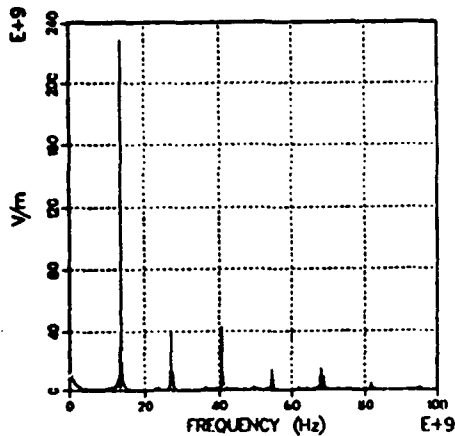MAGIC VERSION: OCTOBER 1990   DATE: 8/14/91
SIMULATION: 8pks 73deg 3.7 8kA 600kV 7keV 510

TIME HISTORY PLOT 3
E1 COMPONENT
AT COORDINATE (310,5)

MAGIC VERSION: OCTOBER 1990   DATE: 8/16/91
SIMULATION: 8pks 73deg 3.7 2kA 600kV 7keV 510

TIME HISTORY PLOT 3
E1 COMPONENT
AT COORDINATE (310,5)

MAGIC VERSION: OCTOBER 1990   DATE: 8/17/91
SIMULATION: 8pks 73deg 3.7 8kA 600kV 7keV 510

TIME HISTORY PLOT 3
E1 COMPONENT
AT COORDINATE (310,5)

– 65 –

SIMULATION: /wide-beam 8pke 75deg 3.1 2kA 600kV 73x310

PHASE-SPACE PLOT OF PZ VS. Z AT TIME: 1.91E-08 SEC
SPECIES: ELECTRON Q/M RATIO: -1.759E+11

Z (m)
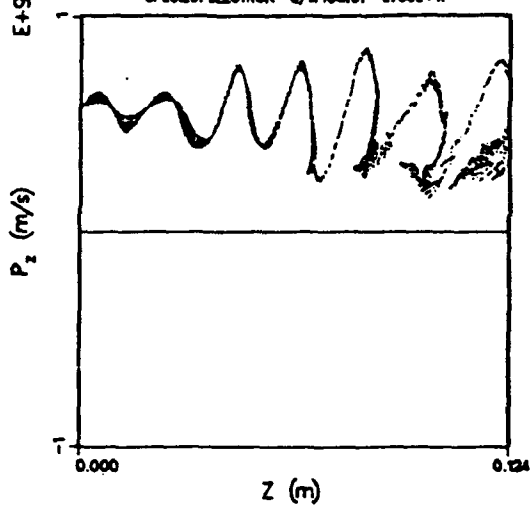
SIMULATION: 8pke 75deg 3.1 2kA 600kV 71x310

PHASE-SPACE PLOT OF PZ VS. Z AT TIME: 1.91E-08 SEC
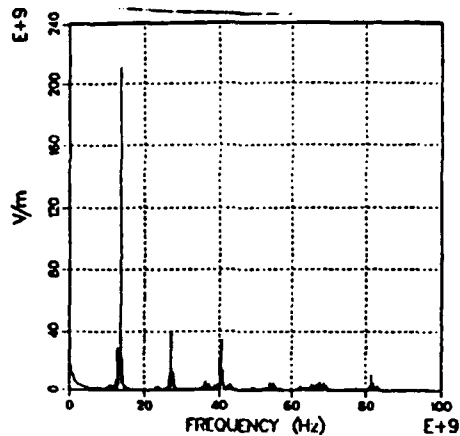SPECIES: ELECTRON Q/M RATIO: -1.759E+11

Z (m)

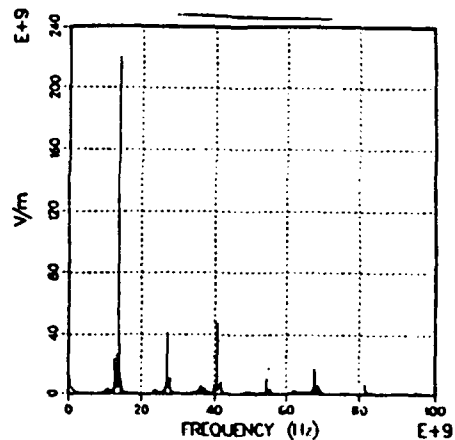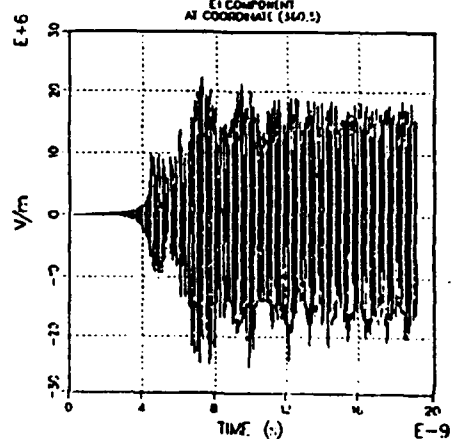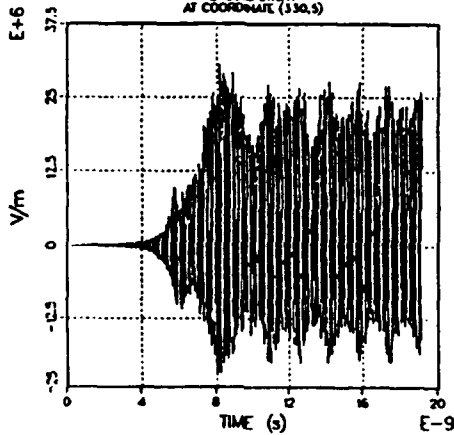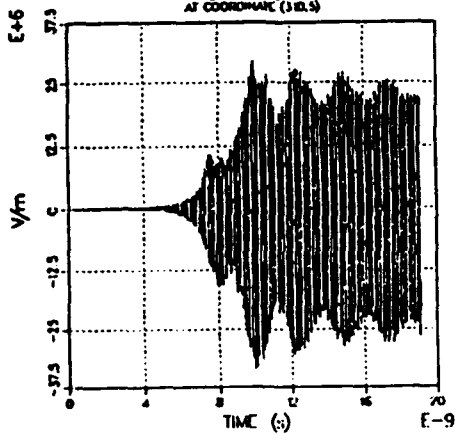AT COORDINATE (310,5)
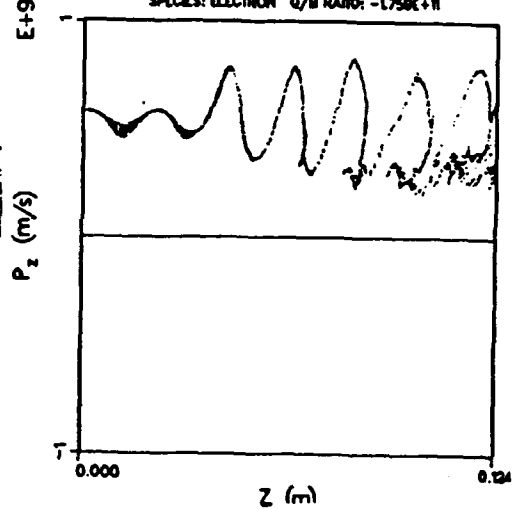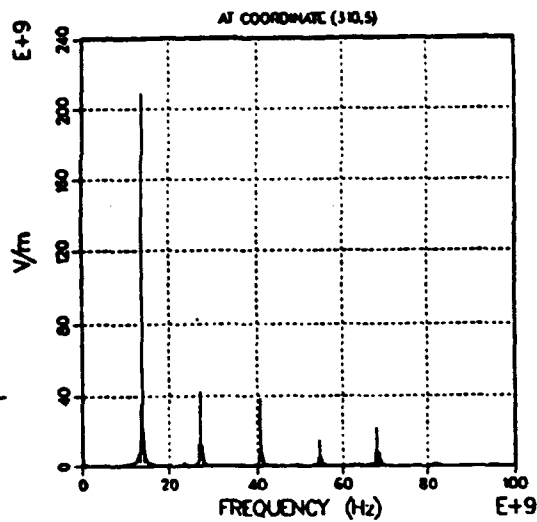
AT COORDINATE (310,5)

MAGIC VERSION: OCTOBER 1990   DATE: 8/21/91
SIMULATION: /wide-beam 8pln 75deg 3.T 2kA 600kV 73x310

MAGIC VERSION: OCTOBER 1990   DATE: 8/16/91
SIMULATION: 8pln 75deg 3.T 2kA 600kV 73x310

TIME HISTORY PLOT 3
E1 COMPONENT
AT COORDINATE (310,5)

TIME HISTORY PLOT 3
E1 COMPONENT
AT COORDINATE (310,5)

CONCLUSIONS

* STARTING CURRENT BETWEEN 1 AND 2 kA

* BACKSTREAMING ELECTRONS AT 8 kA

* BEAM SHEATHS OF 1 AND 2 mm THICKNESS
  GIVE SIMILAR RESULTS

* INCREASING NUMBER OF PERIODS
  DECREASES TURN-ON TIME

* INCREASING BEAM RADIUS DECREASES
  TURN-ON TIME

* FOR THE EIGHT PERIOD STRUCTURE,
  A MAGNETIC FIELD OF 3 TESLA
  PRODUCED FAR BETTER RESULTS
  THAN 1.5 TESLA.

* FREQUENCY OF 14 GHz AGREES WITH
  U of NM DISPERSION CALCULATION.

*** END OF DOCUMENT ***

*** FINAL REPORT TO AFOSR ***

*** GRANT AFOSR-89-0393E ***

Schamiloglu and Gahl,

University of New Mexico